The December 2016 extreme weather and particulate matter pollution episode in the Paris region (France)

Gilles Foret, Vincent Michoud, Simone Kotthaus, J.-E. Petit, A. Baudic, G. Siour, Y. Kim, J.-F. Doussin, J.-C. Dupont, P. Formenti, et al.

Atmospheric Environment 291 (2022) 119386

Contents lists available at ScienceDirect

Atmospheric Environment

journal homepage: www.elsevier.com/locate/atmosenv

The December 2016 extreme weather and particulate matter pollution episode in the Paris region (France)

G. Foret [a,*], V. Michoud [b], S. Kotthaus [c], J.-E. Petit [d], A. Baudic [e], G. Siour [a], Y. Kim [f], J.-F. Doussin [a], J.-C. Dupont [g], P. Formenti [b], C. Gaimoz [a], V. Ghersi [e], A. Gratien [a], V. Gros [d], J.-L. Jaffrezo [h], M. Haeffelin [c], M. Kreitz [i], F. Ravetta [j], K. Sartelet [f], L. Simon [c,k], Y. Té [l], G. Uzu [h], S. Zhang [m], O. Favez [k,n], M. Beekmann [b]

[a] Univ Paris Est Creteil and Université Paris Cité, CNRS, LISA, F-94010, Créteil, France
[b] Université Paris Cité and Univ Paris Est Creteil, CNRS, LISA, F-75013, Paris, France
[c] Institut Pierre Simon Laplace (IPSL), CNRS, École Polytechnique, Institut Polytechnique de Paris, 91128, Palaiseau Cedex, France
[d] Laboratoire des Sciences du Climat et de l'Environnement, LSCE, UMR CNRS-CEA-UVSQ, IPSL, 91191, Gif-sur-Yvette, France
[e] AIRPARIF, Association Agréée de la Surveillance de la Qualité de l'Air en Île-de-France, 7 rue Crillon, 75004, France
[f] CEREA, Ecole des Ponts ParisTech,EdF R&D, Marne la Vallée, France
[g] Institut Pierre-Simon Laplace (IPSL), UVSQ, Université Paris-Saclay, École Polytechnique, Institut Polytechnique de Paris, 91128, Palaiseau Cedex, France
[h] University Grenoble Alpes, CNRS, IRD, INP-G, IGE (UMR 5001), 38000, Grenoble, France
[i] Ecole Nationale de la Météorologie (ENM), Météo-France, 42 avenue Coriolis, 31057, TOULOUSE CEDEX 1, France
[j] LATMOS/IPSL, Sorbonne Université, UVSQ, CNRS, Paris, France
[k] Institut national de l'environnement industriel et des risques (INERIS), Parc Technologique Alata BP2, 60550, Verneuil-en-Halatte, France
[l] Laboratoire d'Etudes du Rayonnement et de la Matière en Astrophysique et Atmosphères (LERMA-IPSL), Sorbonne Université, CNRS, Observatoire de Paris, PSL Université, 75005, Paris, France
[m] Atmo Hauts de France, 59044, Lille, France
[n] Laboratoire Central de Surveillance de la Qualité de l'Air (LCSQA), 60550, Verneuil-en-Halatte, France

HIGHLIGHTS

- Study of an intense winter episode of particulate pollution in the Paris region.
- Exceptional stagnant conditions explain the highest concentrations.
- Organic matter of local origin dominates the chemical composition of the particles with also a strong nitrate component from traffic.
- Significant values of oxidative potential are observed.

1. Introduction

Atmospheric particles are recognized as major air pollutants. Their harmful impact on health is clearly established. Especially long-term effects on respiratory (Chronic obstructive pulmonary disease, lower respiratory infection, lung cancer) and cardiovascular (Ischaemic heart cerebrovascular diseases) segments have been quantified (Cohen et al., 2017). For France alone, the number of premature deaths attributed to Particulate Matter (PM) with aerodynamic up to a diameter of 2.5 μm ($PM_{2.5}$) and NO_2 is about 40,000 per year (Medina et al., 2021) and the associated economic burden is estimated at several tens of billions of euros (Aïchi and Husson, 2015). Even if long term effects are known to be more problematic, the particulate matter exposure over short time scales also impacts mortality and morbidity (Katsouyanni et al., 1996, 2009; Scheers et al., 2018; Choi et al., 2019; Shehab and Pope, 2019), with an increase in mortality between 0.4% and 1.0% per 10 $\mu g.m^{-3}$ $PM_{2.5}$ concentration increase (Katsouyanni et al., 2009).

With about twelve million inhabitants, the Greater Paris region is among the biggest European megacities. Decennial trends recorded by the Airparif air quality monitoring network (AQMN) indicate a slow decrease of the particle mass concentration burden (Airparif, 2020), notably due to the reduction of the emissions of primary particle and gaseous precursors (NOx, SO_2, Volatile Organic Compounds (VOC)) since the 1990s from different activity sectors (transport, industry, energy production and consumption). Still, the annual air quality standard of 10 $\mu g.m^{-3}$ average $PM_{2.5}$ recommended by the WHO (World Health

* Corresponding author.
E-mail address: gilles.foret@lisa.ipsl.fr (G. Foret).

https://doi.org/10.1016/j.atmosenv.2022.119386
Received 28 September 2021; Received in revised form 22 July 2022; Accepted 5 September 2022
Available online 13 September 2022

Organization) is exceeded every year. The PM10 daily average concentration threshold of 50 $\mu g.m^{-3}$ should not be exceeded more than 35 times per year according to European legislation (EU, 2008). This value is generally respected but the WHO recommended values (i.e. less than 3 days per year above 50 $\mu g.m^{-3}$) are not respected. The majority of locations where the daily average PM_{10} concentrations exceeds the legal threshold are monitoring sites located close to major roads. Within the entire Paris region, more than three-quarters of the population is exposed to PM_{10} concentrations above WHO recommendations (Airparif, 2020).

Pollution episodes over dense high-emission urban and suburban areas are also largely controlled by meteorological conditions either causing local build-up of concentrations due to air stagnation or advection of continental pollution plumes originating from densely populated areas located North or East of the Paris region (e.g. Petit et al., 2015). The occurrence of meteorological conditions that can enhance pollution events (such as temperature inversions which reduce vertical dilution of PM) have been found to change in the past. For example, the frequency of winter temperature inversions over the United-States has increased by a factor two according to Hou and Wu (2016), or is expected to do so in future (Horton et al., 2014; Fortems-Cheiney et al., 2017). Vautard et al. (2018) observed a significant increase in the frequency of low monthly wind speeds in wintertime over Western Europe over the last three decades. They point out that December 2016 was among the least windy winter months over this period, and estimate a return-time of such weak flow conditions of ~10 years. They show that this weather pattern associated with extremely low wind speeds coincided with a strong increase in monthly average PM_{10} levels over Western Europe. The 25.4 $\mu g.m^{-3}$ observed in December 2016 significantly exceeds the expected December value based on estimated trends between 2001 and 2016 by the European Environment Agency (EEA) of 16.4 $\mu g.m^{-3}$.

The relative importance of local origins of PM versus particle advection from remote regions for the air quality of the Greater Paris area (hereafter called IDF for Île-De-France region) has been discussed in many studies. For instance, the MEGAPOLI campaigns showed that both summertime and wintertime pollution episodes were generally caused by PM advection from outside of the urban area (Beekmann et al., 2015). Based on annual averages for the 2009–2010 period, 70% of background aerosol mass was estimated to originate from outside of IDF for inorganic but more surprisingly also for organic matter (Beekmann et al., 2015; Petetin et al., 2014). Using a source apportionment approach, Skyllakou et al. (2014) confirmed the prevalence of advected pollution during MEGAPOLI. They showed that Black Carbon (BC) and primary organic aerosol were mainly associated with local sources while sulfate and secondary organic aerosol were mostly associated with remote sources. For a springtime (May/June) pollution event in 2007, Sciare et al. (2010) pointed out the importance of regional sources of PM. A two-year analysis performed at the SIRTA (Site Instrumental de Recherche par Télédétection Atmosphérique) observatory in the southwest suburbs of Paris allowed to investigate different pollution episodes with both local and advected origins in 2011–2013 (Petit et al., 2015). During winter, carbonaceous matter from road traffic and residential heating of local and regional origins are the main PM sources while during spring, ammonium nitrate associated with traffic and agricultural practices dominate (Petit et al., 2015), the latter mainly being advected into the city from rural surroundings. Sartelet et al. (2018) showed that 3–5% of annual average OM (Organic Matter) over the IDF region are from anthropogenic VOC (e.g. toluene, xylene) precursors, while 20–60% of OM are from anthropogenic intermediate and semi volatile organic compound (ISVOC) emissions. ISVOCs mostly originate from combustion sources (traffic, residential sector) (Robinson et al., 2007; Chrit et al., 2018). They have lower volatility than VOCs and SVOCs may partition onto particles, whereas IVOCs may only partition after further oxidation in the atmosphere, which lowers their volatility (Murphy et al., 2014). Ait-Helal et al. (2014) estimated that intermediate volatile organic compounds (IVOCs) contributed to 2–7% of the secondary organic aerosol (SOA) formation during winter and summer MEGAPOLI campaigns conducted at the SIRTA site. During winter episodes, the partitioning of SVOCs onto particles is favored by the low winter-time temperatures. It is not clear whether IVOCs may undergo enough oxidation to be able to partition onto particles: Michoud et al. (2014) showed that due to the larger HONO concentrations measured, the winter-time atmospheric oxidative capacity in Paris is half of that of the summer season. The importance of ISVOCs for winter time air quality over Europe has already been pointed out (Couvidat et al., 2012; Chrit et al., 2018; Giani et al., 2019). Still, although their contribution to winter-time pollution over IDF may be high, potentially even exceeding the annual average estimated by Sartelet et al. (2018), gas-phase emissions of ISVOCs are not yet part of the EU directives on emission reduction.

Oxidative stress is recognized as one of the main processes by which human health is affected by PM (Leni et al., 2020). In addition to PM concentration and composition, the so-called oxidative potential (OP) of PM should be assessed as a complementary metric to estimate the potential health impact of PM. More precisely, OP allows to detect the oxidative stress induced by PM in the human body by measuring the depletion of antioxydants or related species (such like dithiothreitol, DTT or acid ascorbic, AA) present in the epithelial lung fluid (Shiraiwa et al., 2017). OP can be evaluated easily using acellular tests for which PM samplings with filters are put in proxies of the lining lung fluid. Acellular test here means that synthetic lung fluids rather than cultured cells are used to conduct OP measurements which allows much more flexibility in deploying and performing these measurements. Weber et al. (2018) showed that OP is a function of sources driving PM concentrations and few studies have been conducted to estimate OP during intense pollution episodes while no studies have been made until now over the IDF region.

The analysis presented here demonstrates that the pollution episode over the IDF in December 2016 was outstanding both in terms of meteorological conditions and PM levels. To understand what makes this event so exceptional the combination of drivers are characterized carefully using a range of detailed observations.

After introducing the methods, measurement strategy and modelling tools (Section 1), the pollution event is characterized and its drivers are analyzed in the results section (Section 2). Finally, the conclusions (Section 3) put this exceptional episode in the larger context of our understanding of the drivers for severe air pollution risk.

2. Methods, measurement strategy, and modelling tools

This study was carried out by the OCAPI research group (Observation de la Composition Atmosphérique Parisienne de l'Institut Pierre Simon Laplace), established in 2014 in the framework of the EPPI ("Etude de la Pollution Particulaire en Île-de-France") project to better characterize air quality in the IDF. This science-driven program aims at measuring several atmospheric variables simultaneously at four major measurement sites: The dynamical characteristics of the atmosphere, including near-surface and atmospheric boundary layer (ABL) conditions, as well as detailed physical (mass and number size distributions) and chemical composition of particles. It therefore complements Airparif's AQMN, whose objective is operational monitoring. The OCAPI research network monitored PM pollution episodes between November 2016 and December 2019 and studied their determinants. Thanks to a dedicated forecasting group, the EPPI observation strategy for pollution episodes operated based on an alert system.

This section describes the measurement setup numerical models, source apportionment tool, and the resulting datasets used in the study. Additional details on measurement sites, networks and associated online instrumentation and off-line chemical analyses are provided in the supplementary material (Appendix B).

2.1. OCAPI measurement strategy

OCAPI observations were collected at different stations, including the Airparif AQMN, the Creil AQMN site of the Atmo Hauts-de-France, four research platforms of IPSL (SIRTA, Qualair, LISA UPEC and LISA UP) and three Météo-France stations (Trappes, Roissy airport and Parc Montsouris). These measurement sites capture conditions along the rural-suburban0urban gradient across the IDF (Fig. 1).

A range of chemical and meteorological variables were measured at these stations (Table 1). Meteorological observations analyzed in this study include radiosonde profiles measured at synoptic times (00UTC, 12UTC) at the Trappes Meteo France site, profiles of wind speed and direction observed with a Doppler wind lidar at SIRTA, as well as the mixed layer height (MLH) derived from automatic lidar and ceilometer (ALC) observations along a northeast-southwest transect (Roissy, LISA UP, SIRTA). The automatic CABAM algorithm (Kotthaus and Grimmond, 2018) is applied to retrieve MLH at 15 min resolution based on a dynamic decision tree approach. Details on the procedure and uncertainty assessment in the Paris region are provided elsewhere (Kotthaus et al., 2020). Also historical meteorological surface station measurements at Parc Montsouris as well as reanalysis from the national center for environmental predictions (NCEP; Kalnay, 1996) and the ARPEGE model at 0.5° (Pailleux et al., 2014) are used (see Sub-section 2.1).

Hourly PM_{10} measurements were carried out by Airparif at 10 traffic sites, 11 urban/suburban sites and 2 rural sites (Fig. 1) using either TEOM-FDMS 1405-F (Thermo ScientificTM) or beta gauges (BAM 1020, Met OneTM) automated systems. All devices being used by Airparif for gravimetric regulatory measurements of PM meet the applicable French standard (NF EN 12341: "Ambient air – Standard gravimetric measurement method for the determination of the PM_{10} and $PM_{2.5}$ mass concentration of suspended particulate matter") ensuring high-quality data.

Hourly BC concentrations were measured by aethalometers (AE33) at 5 stations (SIRTA, Paris13, A1, BPEst, Bld Haussmann). Two sites were equipped with Aerosol Chemical Speciation Monitors (ACSM) (SIRTA and Gennevilliers) giving access to the hourly non-refractive part of the PM_1 fraction, with organic matter (OM), nitrate (NO_3^-), and sulfate (SO_4^{2-}) used in the study. Additional daily filter samples of aerosols have been collected at SIRTA, Creil and LISA UPEC to obtain the concentrations of the major water-soluble ions (nitrate and sulfate) as well as to elemental and organic carbon (EC and OC, respectively). Most of the chemical speciation data are also part of the so-called CARA ("Caractérisation chimique des particules") program, operated at the national level (Favez et al., 2021). Following the recommendation of Favez et al. (2021) and reference therein, we use a factor of 1.8 to convert OC measurements from filters to OM values analysis. The fraction of BC from fossil fuel use (BC_{ff}) or emitted by wood burning (BC_{wb}) is estimated according to Favez et al. (2021).

OP is analyzed through the measurement of the depletion rate of anti-oxidant compounds as assays with DTT for dithiothreitol (Charrier and Anastasio, 2012; Sauvain et al., 2011; Uzu et al., 2011), AA for acid ascorbic (Bates et al., 2018; Calas et al., 2018), by PM extracts for a given time of reaction. A more detailed description of OP analysis methodology is provided in Appendix C.

It should be noted that some measurement stations do not gather extensive observations continuously. Indeed, it is thanks to the OCAPI initiative that the multi-site strategy is activated for specific periods of interest, whereby enhancing the information content substantially. More precisely when the daily PM_{10} concentration was expected to exceed the threshold of 50 $\mu g.m^{-3}$ for at least two consecutive days at the background stations, enhanced measurement protocols were activated. To determine when these additional measurement capacities should be activated in anticipation of a pollution events, OCAPI interacted closely with the Airparif forecasting division. Alerts on possible

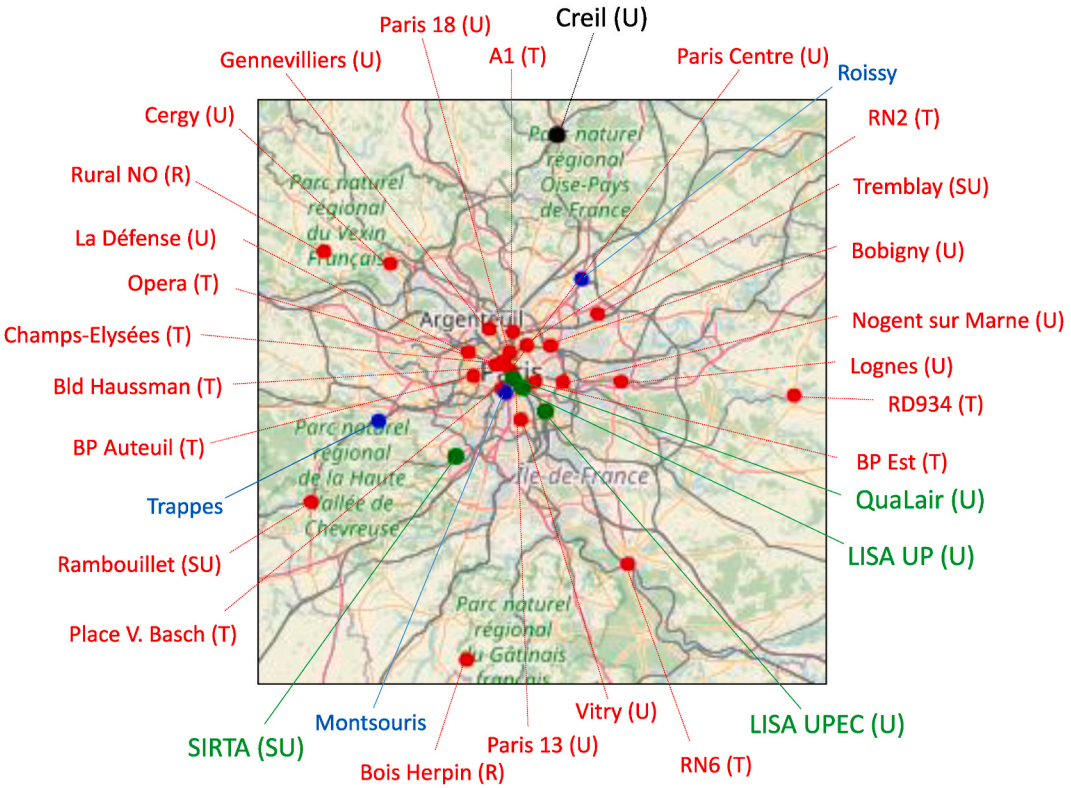

Fig. 1. Locations of measurement sites contributing the OCAPI monitoring program. Red points: Airparif stations measuring PM10 concentrations (and at times BC, cf. Table 1); black points: Creil (Atmo Hauts-de-France); green points: research sites (SIRTA, Qualair, LISA UP, LISA UPEC); blue points: Meteo-France's stations. The source area characteristics of the monitoring stations are indicated as traffic (T) urban (U), suburban (SU) or rural (R). (For interpretation of the references to colour in this figure legend, the reader is referred to the Web version of this article.)

Table 1
Meteorological and chemical variables measured at OCAPI stations (Fig. 1).

Chemical parameters	Site - Instruments	Dynamical parameters	Site - Instruments
PM_{10}	Traffic – TEOM FDMS/ BAM –AIRPARIF (10 stations)	Boundary layer height	Roissy - Ceilometer LISA UP - Ceilometer SIRTA - Ceilometer
	Urban/Sub – TEOM FDMS/BAM – AIRPARIF (11 stations) + FIDAS SIRTA (PM_{10}/$PM_{2.5}$/PM_1)	2D wind speed and direction	SIRTA – Doppler Lidar
	Rural- TEOM FDMS/BAM – AIRPARIF (2 stations)	T° vertical profile	Trappes – radio soundings
OM (Organic Matter)	SIRTA – ACSM (PM_1) SIRTA – Filter ($PM_{2.5}$) Gennevilliers – ACSM (PM_1) Creil – Filter ($PM_{2.5}$) LISA UPEC – Filter (PM_{10})		
NO_3^-(Nitrate)	SIRTA – ACSM (PM_1) SIRTA – Filters ($PM_{2.5}$) Gennevilliers –ACSM (PM_1) Creil – Filter ($PM_{2.5}$)		
SO_4^{2-}(Sulfate)	SIRTA – ACSM (PM_1) SIRTA – Filter ($PM_{2.5}$) Gennevilliers – ACSM (PM_1) Creil – Filter ($PM_{2.5}$)		
BC(Black Carbon/ Elemental Carbon)	SIRTA – AE33 ($PM_{2.5}$) SIRTA – Filter ($PM_{2.5}$) Paris 13 – AE33 ($PM_{2.5}$) Creil – Filter ($PM_{2.5}$) LISA UPEC – Filter (PM_{10})		
CO (Carbon monoxide)	QUALAIR – CO11M analyser		
OP (Oxidative potential)	SIRTA – AA and DTT from filter (PM_{10}) LISA UPEC – AA and DTT from filter (PM_{10})		

upcoming pollution episodes were issues at least two days in advance. In addition, the Meteo-France meteorological forecasts as well as outputs of the three air quality forecasting systems ESMERALDA platform (http://www.esmeralda-web.fr, last access: July 2021), PREV'AIR ("Prévision de la Qualité de l'air") platform (Rouil et al., 2009) and CAMS (Copernicus atmospheric monitoring system; Marécal et al., 2015) were consulted. To activate an intensive measurement period, threshold exceedances needed to be anticipated by at least two out of these three modeling systems.

To put the large number of measurements into the context of the IDF measurement network, their respective representativeness is discussed. Concerning the PM mass, we chose to use the PM_{10} data from Airparif which are most numerous in the region and which are consistent with the fraction used for the OP study. Although the instruments used may vary, they all meet the applicable European standards EN 12341 and EN 16450, respectively.

Concerning the PM chemical speciation, we gathered all available observations to best account for spatial variations and the respective signature according to the source area characteristics (traffic, urban, suburban and rural). This has rather challenging implications for site-to-site and/or instrument-to-instrument comparisons given the stations may differ in terms of the fractions collected, i.e. PM_1 from ACSM devices (SIRTA and Gennevilliers), $PM_{2.5}$ for black carbon measured with AE33 (SIRTA and Airparif stations), and $PM_{2.5}$ from filter-based offline or PM_{10} from chemical speciation (Créteil, SIRTA, and Creil). Regarding the comparison between PM_1 and $PM_{2.5}$ measurements, it is assumed that $PM_{2.5}$ is predominately included in the submicron aerosol fraction in Europe and the IDF region more specifically (Ramgolam et al., 2009). In the present study, the information provided by FIDAS measurements at SIRTA confirms that the $PM_1/PM_{2.5}$ ratio is 0.92 and the correlation coefficient (R) is 0.998. At SIRTA, PM_1 ACSM measurements can be compared to $PM_{2.5}$ from chemical analysis of the filters. The results (Table 3) from the two methods are consistent for all species observed (nitrate, sulfate and organic matter), with concentrations obtained from $PM_{2.5}$ filter-based measurements only slightly higher (typically about 10% on average) than those retrieved from the ACSM for submicron aerosols. Based on these findings, it is here assumed that differences between PM_1 and $PM_{2.5}$ are small in terms of both mass and chemical speciation across the entire IDF region.

Concerning discrepancies between the $PM_{2.5}$ and PM_{10} fractions during the period analyzed here, it should be noted that mass ratios between these two fractions are higher at the rural, suburban and urban stations (with 0.87, 0.78, 0.77, 0.77, 0.75, 0.74, 0.73, at SIRTA, Bois Herpin, Rambouillet, Paris Centre, Gennevilliers, Vitry and Bobigny stations, respectively and 0.55, 0.59, 0.61, 0.66 at the traffic sites A1, Auteuil, RN6, and BPEst, respectively). These lower ratios at traffic stations are likely associated with the dominant influence of coarse particles' emissions from abrasion (road, brakes, and engine) and resuspension processes. Moreover, for all these stations (except RN6), correlation coefficients between the two size fractions are greater than 0.9 showing that the temporal dynamics are similar for the two fractions at all available sites during the studied period.

In the following, the corresponding size fraction is systematically stated for each measurement, keeping in mind the limitations potentially influencing the analysis.

2.2. Source apportionment of carbonaceous aerosols

Positive Matrix Factorization (PMF, Paatero and Tapper, 1994) was used to perform source apportionment of submicron organic aerosols (OA) from ACSM data at SIRTA, using the SoFi tool (Canonaco et al., 2013). This methodology was previously applied to several years of ACSM data at SIRTA (from end of 2011 to early 2018; Zhang et al., 2019). Briefly, the analysis enables the separation of the OA component into different sub-fractions - referred to as OA factors - based on the time-dependent and partial covariation of some mass-to-charge ratios (m/z's). These m/z's constitute the spectral fingerprint of the measured submicron aerosols. As applied here, the PMF analysis allows for a deconvolution the total measured OA mass spectra into a combination of several factors corresponding to different specific mass spectra. The obtained factors describe the types of OA and give insights on their sources or formation pathways. At SIRTA, various studies showed that the main OA factors are generally composed of two primary factors: Hydrocarbon-like Organic Aerosols (HOA) mostly from traffic, Biomass Burning OA (BBOA), and two secondary factors containing Oxygenated OA: Less Oxidized OOA (LO-OOA) and More Oxidized OOA (MO-OOA). These OOA generally mainly originate from secondary processes (Petit et al., 2014; Zhang et al., 2019).

2.3. Regional chemical transport models

To assist the characterization of the spatial dynamics of the pollution event, numerical modeling is incorporated. It further allows for the determination of relevant source regions (local or regional/continental). The regional chemistry transport models (rCTM) CHIMERE and POLAIR3D/Polyphemus have been used in numerous studies for modelling air quality over the Île-de-France region with intense model/measurement comparisons during the MEGAPOLI campaigns (e.g. Royer et al., 2011; Couvidat et al., 2013; Wang et al., 2014; Petetin et al., 2014; Kim et al., 2015; Zhang et al., 2013, 2015; Zhu et al., 2016a, 2016b; Sartelet et al., 2018).

Table 2 summarizes the main technical characteristics of these rCTM and provides details on the set-up used in this study. To consider local but also regional and continental emissions and transformations of incoming air masses, nested simulations are used with a final horizontal resolution of 2 km (POLAIR3D/Polyphemus) and 3 km (CHIMERE) over the IDF. The building emission inventories, anthropogenic and biogenic,

Table 2
Details on numerical simulation using the regional chemical-transport models CHIMERE and POLAIR3D/Polyphemus.

	CHIMERE	Polyphemus/Polair3D
Simulation period	2016/11/15 to 2016/12/14	2016/11/29 to 2016/12/13
Horizontal resolution with 3 nested domains	Europe 27 km – France 9 km – Paris region 3 km	Europe 0.5° – France 0.1° – Paris region 0.02°
Vertical resolution	8 (σ,p) levels – Surface to 500 hPa	14 levels – Surface to 12 km
Anthropogenic emissions	Gridded emissions in 0.5° as used in EMEP models for the year 2014 (www.ceip.at; Vestreng, 2003)	Gridded emissions in 0.5° as used in EMEP models for the year 2013 (www.ceip.at; Vestreng, 2003)
Biogenic emissions	MEGAN – Guenther et al., 2006	MEGAN – Guenther et al., 2006
Meteorology	WRF 3.7 (Skamarock et al., 2008) forced by NCEP/GFS FNL analyses (https://doi.org/10.5065/D6M043C6)	WRF 3.6.1 (Skamarock et al., 2008) forced by NCEP/GFS FNL analyses (https://doi.org/10.5065/D6M043C6)
Chemistry/aerosol	MELCHIOR2/VBS Cholakian et al. (2018)	CB05 (Yarwood et al., 2005; Kim et al., 2011) SIREAM (Debry et al., 2007) SOAP (Couvidat and Sartelet, 2015)
Chemical boundary conditions	LMDz_INCA (Hauglustaine et al., 2014) and GOCART (Ginoux et al., 2001) climatologies	MOZART-4 (Emmons et al., 2010) https://doi.org/10.5194/gmd-3-43-2010

use slightly different methods but are based on the same input data (respectively the European Monitoring and Evaluation Programme, EMEP and the Model of Emissions of Gases and Aerosols from Nature, MEGAN). The meteorological forcing is very similar for the two models with by regional simulations undertaken with the weather research and forecasting model (WRF) which are again forced by the NCEP global model. A more detailed description of the model setup is outlines in Appendix C.

3. Results

3.1. Description and analysis of the pollution event

During December 2016 a strong pollution event occurred in the IDF region, both in terms of intensity and duration, between 30th November 2016–17th December 2016 (Fig. 2). According to the PM_{10} concentrations the event can be sub-divided into three distinctive periods, each defined by consecutive days on which hourly median PM_{10} concentrations reach values $\geq$ 50 $\mu g.m^{-3}$ (periods PI and PII) or $\geq$40 $\mu g.m^{-3}$ (period PIII) at the urban background stations.:

1 PI (2016/11/30–2016/12/02)
2 PII (2016/12/05–2016/12/07)
3 PIII (2016/12/14–2016/12/17)

During the entire pollution event, daily average PM_{10} concentrations exceeded the alert threshold (>80 $\mu g.m^{-3}$) and the warning threshold (>50 $\mu g.m^{-3}$) on four days each (alert: 01, 02, 06 and 07 of December; warning: November 30 and December 5, 8 and 15) (Airparif, 2017). During PI, the average PM_{10} concentrations over all hourly values was 92 $\mu g.m^{-3}$ across the traffic sites and 82 $\mu g.m^{-3}$ at the urban sites (Table 3).

PI was a remarkable period in terms of observed PM_{10} at almost all stations, independent of the source area class (traffic/(sub)urban/rural). Further were very high NO_2 concentrations observed across the IDF region during PI peak hourly values reaching ~200 $\mu g.m^{-3}$ (1st December). PII exhibits high average PM_{10} concentrations (although slightly lower compared to PI) with mean values of 82 $\mu g.m^{-3}$ at traffic stations and 63 $\mu g.m^{-3}$ at urban background sites (Fig. 2a and Table 3), i.e. well above daily regulatory threshold 50 $\mu g.m^{-3}$. During PIII, PM_{10} concentrations are generally lower (Table 3), but hourly values were still above 50 $\mu g.m^{-3}$ at the traffic stations (Fig. 2a). The range of PM_{10} concentrations (max minusmin within brackets) observed at the different station types (Table 3) reveals that traffic sites experience the greatest variability (especially in PIII period). However, it should be noted that during the PII period the range of concentrations observed at (sub) urban sites is of the same order of magnitude as that at traffic sites and even exceeds this variability for the PI period. For the PI period, this probably indicates a strong mixing of the polluted air masses over the whole region.

To understand the implications of mixing and atmospheric transport for high PM_{10} concentrations and their variability, meteorological and dynamical conditions are analyzed. As can be seen from the ERA5 reanalyses geopotential height anomaly at 500 hPa (Fig. 3), December 2016 has a strong positive anomaly above northern France and the Be-Ne-Lux region as derived against the 30-year climatology, highlighting n anticyclonic blocking situation over Northern France.

The day-to-day evolution of the anticyclonic system over the PI and

Table 3
Median hourly PM_{10} concentrations with range [max minus min] in brackets. Chemical PM components median concentrations: Black carbon (BC), Organic Matter (OM); Nitrate (NO_3^-); Sulfate (SO_4^{2-}). Concentrations derived from filter analysis are daily totals while ASCM and AE33 mean hourly values. The median hourly BC-to-sulfate ratio is calculated from AE33 and ACSM measurements at SIRTA Entire event: 2016/11/28–2016/12/17); PI: 2016/11/30–2016/12/02); PII: 2016/12/05–2016/12/07; PIII: 2016/12/14–2016/12/17.

		Entire event	PI	PII	PIII
	Site (or type)/instruments				
PM_{10} $\mu g.m^{-3}$	**Traffic** –TEOM-FDMS/BAM –AIRPARIF (10 stations)	59 [45]	92 [71]	82 [55]	56 [38]
	Urban/Suburban– TEOM FDMS/BAM – AIRPARIF (11 stations)	44 [38]	82 [86]	63 [54]	39 [30]
	Rural- TEOM FDMS/BAM – AIRPARIF (2 stations)	25 [11]	43 [15]	34 [21]	25 [15]
OM $ug.m^{-3}$	SIRTA – ACSM (PM_1)	12	19	19	12
	SIRTA – Filter ($PM_{2.5}$)	14	22	24	15
	Gennevilliers – ACSM (PM_1)	21	36	30	19
	Creil – Filter ($PM_{2.5}$)	29	62	41	22
	LISA UPEC – Filter (PM_{10})	20	48	26	12
NO_3^- $\mu g.m^{-3}$	SIRTA – ACSM (PM_1)	5	9	8	5
	SIRTA – Filters ($PM_{2.5}$)	6	10	10	5
	Gennevilliers –ACSM (PM_1)	10	12	13	8
	Creil – Filter ($PM_{2.5}$)	7	15	11	5
SO_4^{2-} $\mu g.m^{-3}$	SIRTA – ACSM (PM_1)	1.3	1.8	1.7	1.6
	SIRTA – Filter ($PM_{2.5}$)	1.4	1.8	1.9	1.8
	Gennevilliers – ACSM (PM_1)	1.4	1.8	1.6	1.7
	Creil – Filter ($PM_{2.5}$)	1,8	3.0	2.5	1.8
BC $ug.m^{-3}$	SIRTA – AE33 ($PM_{2.5}$)	2.8	4.8	4.6	3.4
	SIRTA – Filter ($PM_{2.5}$)	2.2	4.2	3.5	2.2
	Paris 13 – AE33 ($PM_{2.5}$)	4.8	12.2	6	3.7
	Creil – Filter ($PM_{2.5}$)	3.7	5.7	4.7	2.4
	LISA UPEC – Filter (PM_{10})	2.7	5.6	3.3	1.9
BC/SO_4^{2-} ($ug.m^{-3}$/$\mu g.m^{-3}$)	SIRTA – AE33/ACSM (PM_1)	2.2	2.7	2.7	2.1
	SIRTA – Filter ($PM_{2.5}$)	1.6	2.3	1.8	1.2
	Creil – Filter($PM_{2.5}$)	2.1	1.9	1.9	1.3

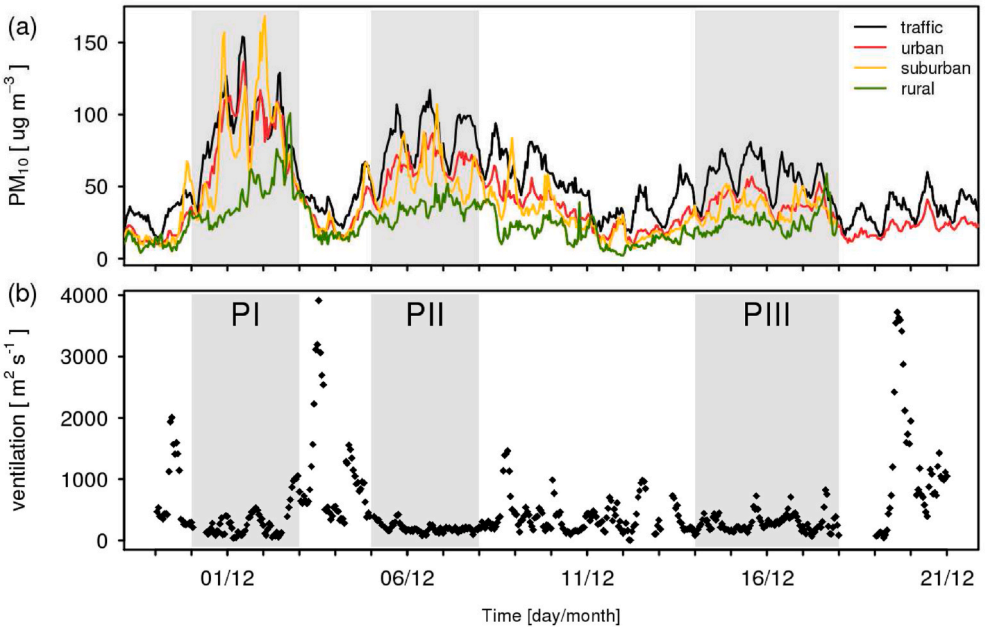

Fig. 2. Hourly (a) PM_{10} concentrations (ug.m^{-3}) averaged over the AIRPARIF operational monitoring network (10 traffic stations; 9 urban stations; 2 suburban stations; 2 rural stations) and (b) ventilation. Shaded areas indicating the three main pollution periods (PI, PII and PIII as defined in the text).

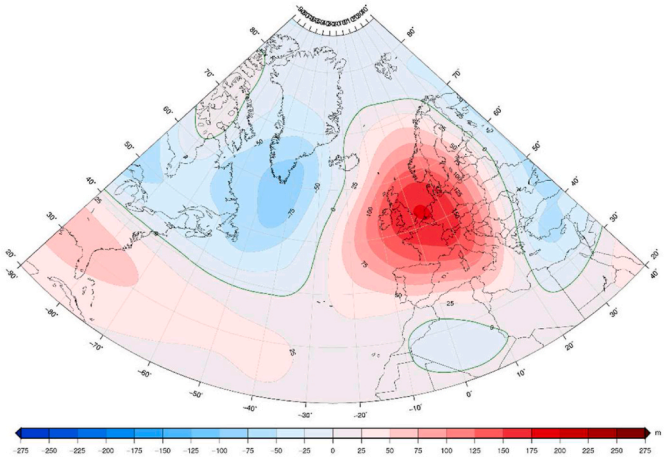

Fig. 3. Anomaly of geopotential height (in meters) at 500 hPa for December 2016 compared to the 1981–2010 climatology calculated from ERA5 (Hersbach et al., 1999).

PII periods as analyzed from the ARPEGE model output (Fig. 4) highlights how the position of the anticyclone varies with respect to the IDF region. It can be seen in particular that the highest pressures and the weakest winds are observed during the PI and PII periods. The vertical profile of horizontal wind speeds observed by the Doppler wind lidar at the SIRTA confirms this evolution: especially PI is characterized by calm winds (generally below 2 m s^{-1}) from variable directions up to about 300 m above ground level (Fig. 5). In the morning of December 1st, wind speeds were only about 1 m s^{-1}. Between these three periods of weak winds, stronger winds are observed, which increases the dispersion of air masses and therefore the reduction of pollutant concentrations in the boundary layer.

During PI, cloud-free nights allowed for strong radiative cooling of the surface. In combination with the low wind speed and large-scale subsidence, this resulted in very strong atmospheric stratification (as observed by Trappes radiosoundings, Figure A1), especially at night (up to +6 °C between 2 m and 30 m air temperature in the night 30/11-01/12). Due to the low buoyancy and strong capping inversion, boundary layer heights remained extremely shallow as illustrated by the ALC attenuated backscatter profile observations and derived MLH (Fig. 6). MLH remained below 200–300 m even during day time, with very similar ABL dynamics at the central urban and suburban locations. This is in accordance with the strong temperature inversion at 200–300 m (Figure A1). Days with shallow MLH (Fig. 6) coincided with low wind speeds in the ABL profile (Fig. 5).

To combine the effects of low horizontal transport and reduced vertical mixing, the ventilation index (product of 2 m wind speed and MLH) is calculated (Fig. 2b) as a proxy of the air flux (in volume) advected out of the considered area (in this case around the SIRTA site). It is clear from Fig. 2b that the periods of low ventilation correspond to the periods of peak PM_{10} concentrations. While shallow MLH and low ventilation index do not always lead to high levels of near-surface PM_{10} concentrations (Fig. 7), they present as a necessary condition for the formation of such severe pollution episodes as pollution levels usually reduce significantly whenever ventilation increases. Given general trends of horizontal wind speed and MLH are driven in large parts by the synoptic conditions, the ventilation index calculated at the suburban SIRTA observatory is mostly representative for the entire IDF study region. It is hence not surprising that PM_{10} concentrations at all Airparif measurement sites confirm that low ventilation levels are clearly linked to the formation of severe particle pollution levels (Fig. 7).

Spatial variations of pollution concentrations during the PI and PII periods are investigated based on simulations with the regional chemistry transport model CHIMERE. The modelled daily average PM_{10} concentrations are broadly consistent with observations (Fig. 8) and reproduce the response of pollution concentrations to the meteorological conditions. While the stagnant flow during PI encourages local accumulation of pollutants in and around the city center with higher PM_{10} concentrations over the eastern part of Paris, the slightly stronger winds from the south-east lead to the formation of a weak pollution plume downwind of the city center during PII. This creates strong spatial gradients within the urbanized area. Very similar features are obtained from POLAIR3D/Polyphemus simulations (not shown) adding robustness to these results.

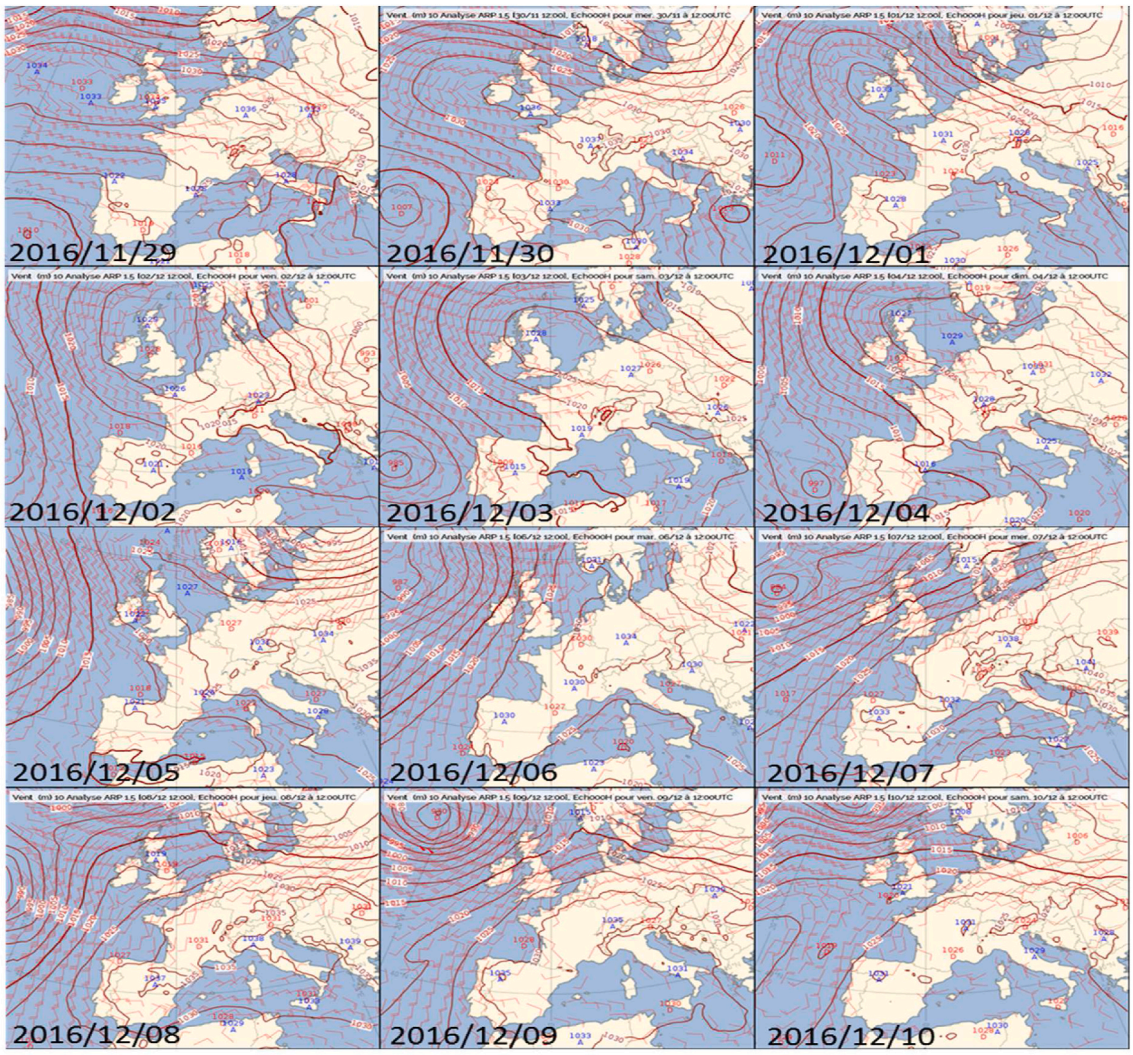

Fig. 4. Surface pressure and 10 m winds from ARPEGE analysis for the period ranging between November 29th and December 10th, 2016 (Source Meteo-France).

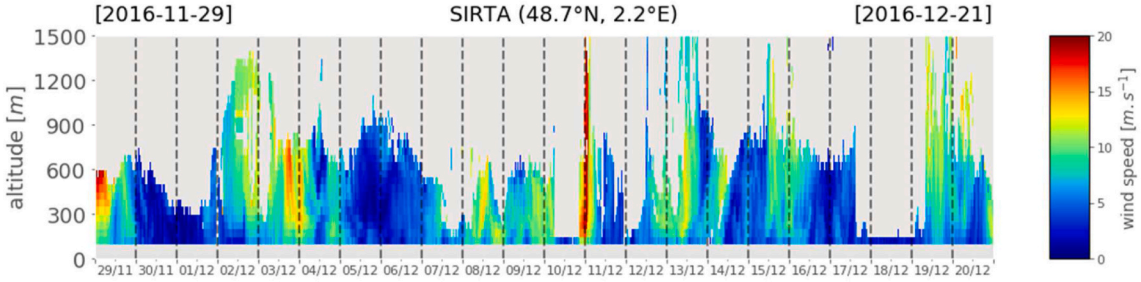

Fig. 5. Time series of vertical profile of horizontal wind speed measured by the WLS70 Doppler lidar installed at SIRTA observatory between November 29, 2016 and December 21, 2016.

3.2. Exceptional character of the event

In this section the December 2016 pollution episode is put into context to the literature to highlight its exceptional character, both in terms of PM concentrations and meteorological conditions. PM_{10} concentrations over the IDF region area exhibit decreasing trends since 2000 (Airparif, 2020). Here, multi-year observations (2007–2020) at the Airparif stations are used as a reference as semi-volatile matter started to be systematically accounted for in 2007, using filter dynamics measurement systems (FDMS) upstream the gravimetric reference monitoring tapered element oscillating microbalances, TEOM (Favez et al., 2007).

Fig. 9 shows boxplots of hourly PM_{10} concentrations at several Airparif stations over the 14 years (2007–2020) in comparison to concentrations measured during PI. It shows that PI is among the most severe pollution episodes observed over the whole 14-year period, with especially high pollution levels in the eastern part of the domain (Tremblay, Lognes, Paris Centre and BPEst) as also seen in the numerical simulations (Fig. 8). Maximum hourly PM_{10} concentrations observed at the above mentioned stations during the PI period are the highest of the

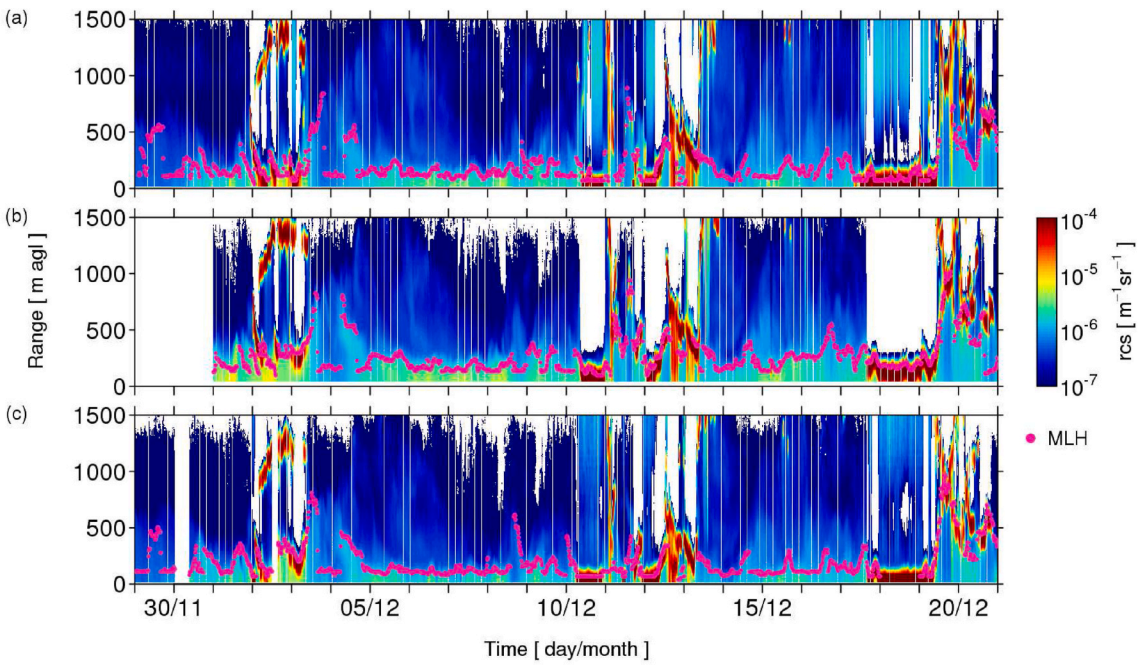

Fig. 6. Time series of vertical profiles (height above ground level, agl) of range-corrected signal (rcs) attenuated backscatter signal (color bar) measured with automatic lidars and ceilometers (Vaisala CL31) ceilometer installed at (a) SIRTA Observatory (top), (b) LISA UP station (middle), and (c) Roissy Airport (bottom) between November 29, 2016 and December 20, 2016. Symbols show derived mixed layer height (MLH) at 15 min resolution. (For interpretation of the references to colour in this figure legend, the reader is referred to the Web version of this article.)

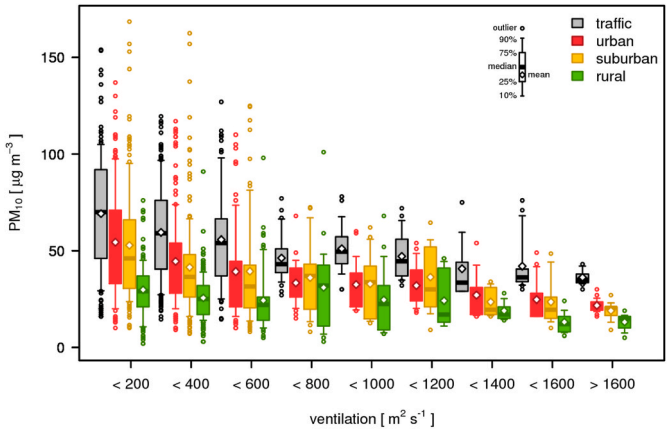

Fig. 7. Boxplots of the hourly PM_{10} concentrations (from Airparif measurements) classified as a function of the hourly ventilation index calculated at SIRTA for the period 2016/11/29 to 2016/12/20. Outliers are values > 90th percentile or <10th percentile, respectively.

recorded series since 2007 (with more than 120000 hourly samples available at each station). For stations A1 and Nogent-sur-Marne, the maximum values observed correspond to a percentile higher than 0.999 with only one other higher value observed at this station over the study period. For this period (PI), hourly PM10 concentrations up to 200 µg. m^{-3} were observed at (sub) urban sites like Bobigny, Tremblay, Paris Centre, Nogent-sur-Marne which are higher than those measured at traffic sites like RN2 Pantin and even A1 (usually the most polluted site of the IDF region). The daily average CO concentrations of respectivey 1.15 ppm (2016/12/01) and 0.78 ppm (2016/12/01) observed at the Qualair station in the center of Paris of and 02 correspond to the 99.9 and 99.8 percentiles of the 2014–2020 period. The daily maximum of CO observed on 2016/12/01 (2.08 ppm) is even the highest hourly value observed between 2014 and 2018 at this site. figure A3 shows the extremely high values observed during the episode compared to the 2014–2018 period.

This unusual pollution event is explained by the exceptional meteorological situation encountered during this period. Vautard et al. (2018) found the decadal pollution maximum corresponds to a 10-year return time of the meteorological conditions encountered in December 2016. Meteorological conditions in December 2016 were exceptional over Western Europe as a blocking anticyclonic system persisted for about three weeks (from 30 Nov-17 Dec). Monthly mean surface winds over Western Europe were among the lowest observed of the last three decades according to Vautard et al. (2018).Pressure anomalies from NCEP reanalysis (Kalnay, 1996, http://iridl.ldeo.columbia.edu/, last access: July 2021) are above the 99th percentile (January 1949–December 2018 base period) for Western Europe, and the 99.8th percentile for the Paris grid point. In accordance with the synoptic situation, surface meteorology was characterized by a positive surface pressure anomaly (the 1029.9 hPa December average is the highest monthly mean value since 1958), low wind speeds (average of 2.2 m s^{-1} for December 2016 among the 5 lowest values for winter months), reduced precipitation and very stable conditions (as recorded at the Parc Montsouris inside Paris city a long term measurement site of Meteo-France and the operational radiosoundings).

Consistent with this synoptic blocking, extremely low values of the ventilation index occurred in December 2016 compared to the 2010–2017 period (Fig. 10). This underlines the poor pollutant dispersion contributing to the exceptionally high PM concentrations observed.

To summarize, although long-term PM concentrations over IDF in general experience a decreasing trend, the pollution event during the PI period was the most intense since 2007. The exceptionally stable synoptic situation associated to very low air masses dispersion is a key driving factor.

3.3. *Particle chemical composition and sources*

To understand the sources contributing to the evolution of the pollution measurements from multiple-sites (Table 1) are analyzed to characterize the particle composition over the region.

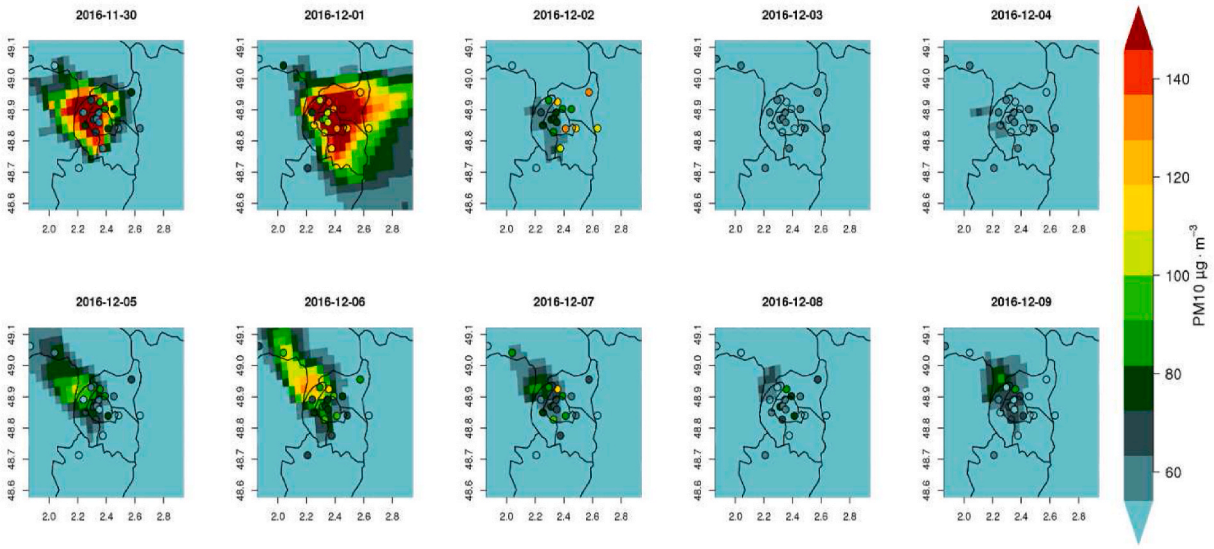

Fig. 8. Mean daily PM_{10} surface concentrations (ug.m^{-3}) from CHIMERE simulations between November 30th and December 9th, 2016. Circles represent Airparif's stations (Fig. 1) coloured by the observed daily mean values of PM_{10} concentrations.

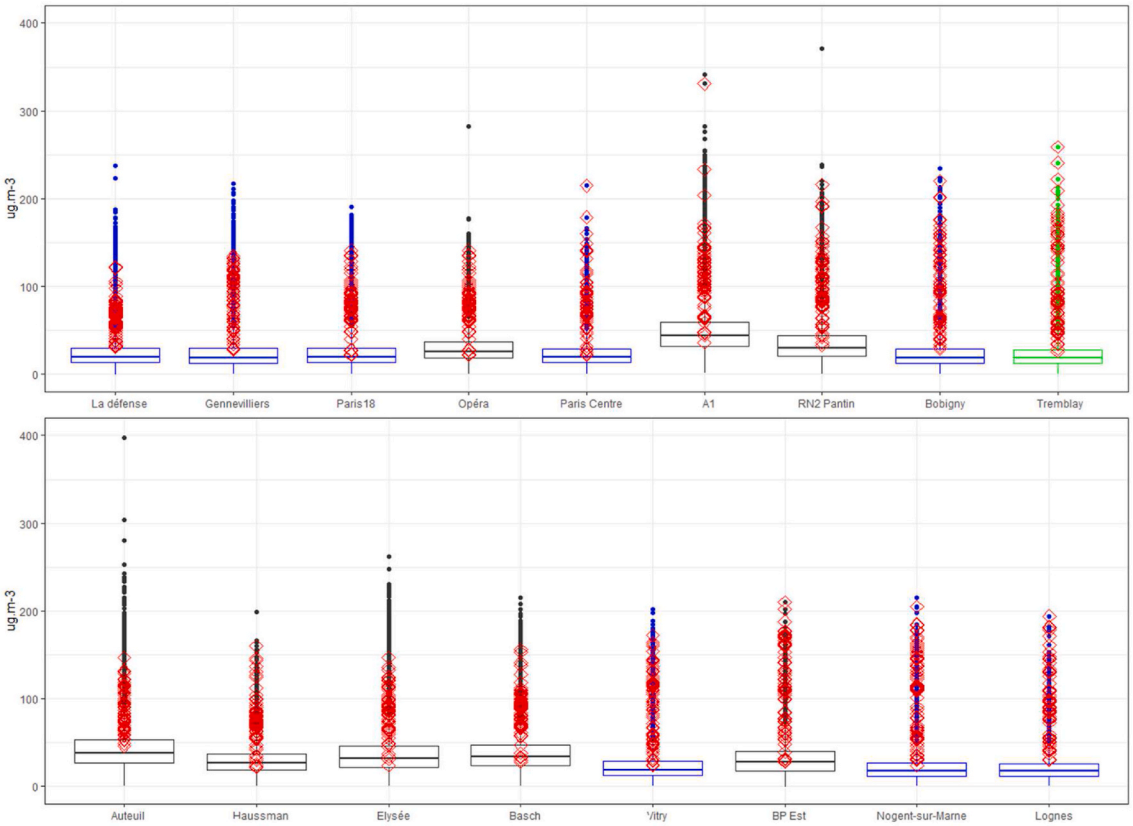

Fig. 9. Boxplots of hourly PM_{10} concentrations (ug.m^{-3}) at selected Airparif stations (2007–2020). Boxplots of traffic, urban and suburban stations are respectively written in black, blue and green. Red diamonds represent the values measured during the PI period (2016/11/30 to 2016/12/02). The positioning of the boxplots on the figure is roughly organized following their North to South and West to East locations. (For interpretation of the references to colour in this figure legend, the reader is referred to the Web version of this article.)

3.3.1. *Carbonaceous aerosols*

During the whole event, OM dominates the aerosol composition as shown in Table 3. Highest concentrations are observed in the urban area with largest average values of 21, 29 and 20 µg.m^{-3} at Gennevilliers (PM_1 of ACSM), Creil (PM2.5 filters) and LISA UPEC (PM10 filters), respectively for the whole event compared to less than 14 µg.m^{-3} (filters) and 12 µg.m^{-3} (ACSM) at the suburban SIRTA site located in the Southwest of Paris (Fig. 1). Again, at the urban sites, highest OM concentrations are observed during PI in accordance with the highest PM_{10} concentrations (Sub-section 2.1). Hourly OM concentrations observed at Gennevilliers during the PI period (hourly maximum value up to 75 µg. m^{-3}) are among the highest measured at this station with an ACSM

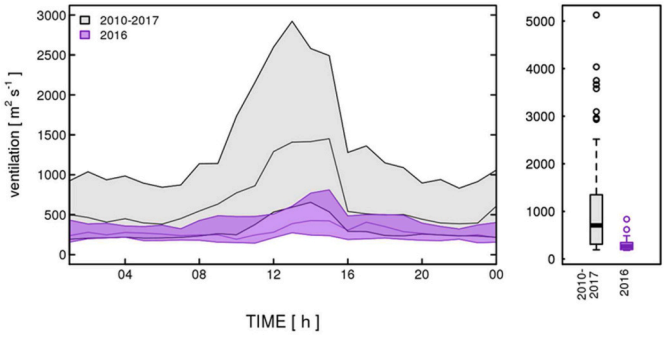

Fig. 10. Median diurnal cycle of ventilation index for the period 2010–2017 (with shading the associated inter quartile range) and for December 2016. Boxplots are calculated using 24h daily means.

(PM_1) for the recent 2016–2020 period (Fig. 11). On the contrary, OM concentrations at the suburban SIRTA site vary less between the event periods (Table 3 and Figure A2). At this station mean OM concentration (12 μg.m^{-3}) represent up to 50% of the PM_1 fraction (Figure A2 and Table 1). Higher concentrations (19 μg.m^{-3}) are observed during the PI and PII periods (same finding is made from filter measurements). Such OM concentrations for PM_1 fractions are consistent with those generally observed at SIRTA for typical local pollution events (Petit et al., 2015). The gradient between the Paris city and SIRTA is also consistent with the fact that the stagnant flow is more concentrated over the denser urban environment in PI and was slightly advected downwind towards the Northwest during PII (see Fig. 8).

Year-round traffic emissions and wintertime residential wood burning are known to be the major local sources of carbonaceous particles in IDF (e.g., Favez et al., 2009).

Zhang et al. (2019) present the source apportionment of submicron organic aerosols (OA) at SIRTA from end of 2011 to early 2018. Fig. 12 shows the concentrations of the four apportioned factors during the December 2016 pollution event. The main feature lies in the dominance of the contribution of primary OA (POA=HOA + BBOA) during PI (69% of OA ± 8%) and PII (66% of OA ±14%), exceeding 80% during specific hours. These values are significantly higher than the average POA contribution for December months (41%, calculated over the 2012–2018 period). More specifically, BBOA and HOA during December 2016 were higher by a factor of around 2.5 compared to other December values, thus highlighting a strong anomaly also regarding the chemical composition of PM. Moreover, they contrast with the sporadic character of POA for high PM concentrations, as shown in Petit et al. (2015), since POA was the main component of OA during several days in a row. Finally, it should be noted that the relative co-variation of HOA and BBOA during the pollution event contrasts with the low r^2 value between BC_{wb} and BC_{ff}, which, as reported in Petit et al. (2014), suggests that source attribution from PMF analysis may be more arduous in the case of strong wood-burning emissions.

BC concentrations show similar features as the OM concentrations (Table 3). Generally higher BC values were observed at urban sites (Paris13, Creil, LISA UPEC) compared to the suburban SIRTA site, especially for PI. During this period, average BC concentrations exhibit highest values (mean concentration of 12.2 μg.m^{-3} and a maxima hourly value of 26.8 μg.m^{-3} on 1st December at Paris13). Fig. 11 also shows that hourly BC values observed at Airparif sites (either traffic or urban background situations) are the highest observed for the 2016–2020 period. The event-mean BC concentration at SIRTA is 2.8 μg.m^{-3} (4.8 and 4.6 μg.m^{-3} for PI and PII periods and 3.4 μg.m^{-3} for PIII period.) with hourly peak values reaching 12 μg.m^{-3} (during PI, on December 1st at 9 a.m.). Hourly values during the PI and PII periods are quite high compared to the long-term winter-time (since 2011) average BC concentration at SIRTA of <1 μg.m^{-3}, and also exceed the mean BC concentrations (4 μg.m^{-3}) observed during high PM episodes analyzed previously (Petit et al., 2015). Similar conclusions can be drawn from filter measurements made at SIRTA (Table 3).

Although BC levels at the Paris13 station are greater than BC concentrations recorded at SIRTA, the estimated relative contribution of wood burning (BC_{wb}) compared to the relative contribution of fossil fuel (BC_{ff}) is fairly similar at the two sites (Table 4) with little temporal variations. Based on these BC observations, primary OM can be estimated following Favez et al. (2021): the primary fraction of OM is estimated by the sum of the BC_{ff} fraction multiplied by 2 and of the BC_{wb} fraction multiplied by 13. It should be noted that the factor 2 to convert BC_{ff} to primary PM associated to traffic emissions seems not very variable (Aiken et al., 2008; El Haddad et al., 2009) while for wood burning the factors can be very different from one places to another as discussed by Favez et al. (2021). Here, the extrapolated values (13, 21, 23 and 15 μg.m^{-3}) are consistent with averaged OM concentrations measured at SIRTA by ACSM and filters elsewhere for all periods analyzed (whole event, PI, PII and PIII, respectively). Then considering the classical error bars of the used OM/BC factors (about a factor of 1.5 following LCSQA, 2015), this analysis suggests that organic matter is mainly of primary origin during this event. This finding is in good agreement with outputs obtained from OA source apportionment at SIRTA. Also, it can be reminded that $PM_{2.5}$ and PM_1 concentrations at SIRTA are relatively similar along the measurements periods with a $PM_1/PM_{2.5}$ ratios below 0.9 allowing to compare ACSM, filters and AE33 measurements for OM and BC with low biases associated to different sampling conditions.

The POLAIR3D/Polyphemus simulations confirm results of the observations-based analysis with a predominant primary and local contribution from both wood burning and traffic to OM, the major PM

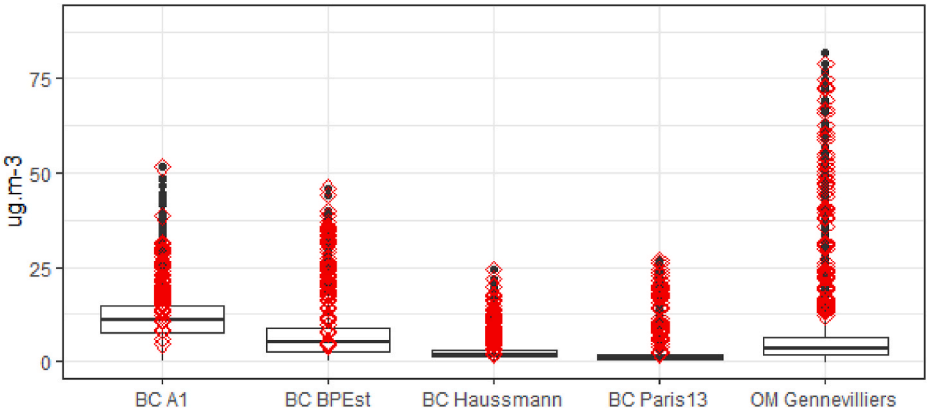

Fig. 11. Boxplots of OM (Gennevilliers) and BC (A1, BPEst, Haussmann, Paris13) concentrations measured during the 2016–2020 period. Red diamonds indicate the values measured during the PI period. (For interpretation of the references to colour in this figure legend, the reader is referred to the Web version of this article.)

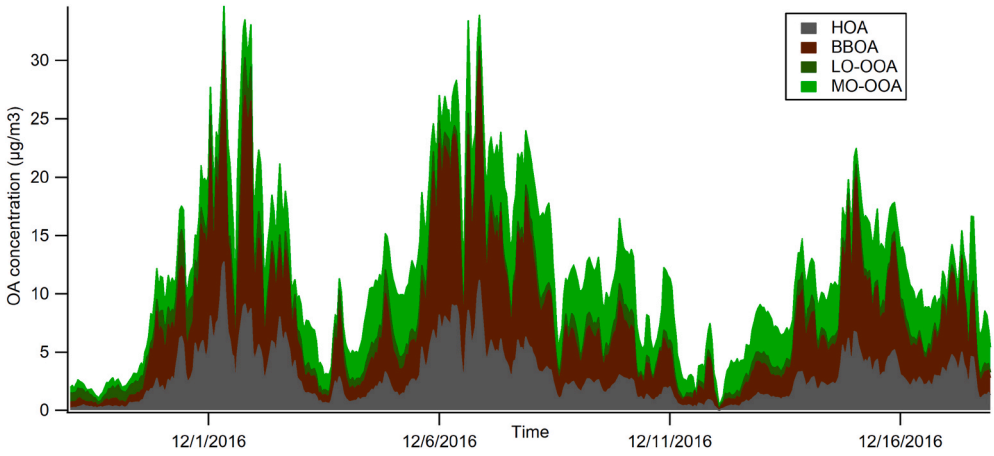

Fig. 12. Contribution of OA factors to the total OA concentration between November 28, 2016 and December 17, 2016.

Table 4
Hourly averaged black carbon concentrations (ug.m^{-3}) from fossil fuel (BC_{ff}) and wood burning (BC_{wb}) observed at SIRTA (ACTRIS) and Paris 13 (AIRPARIF) stations with an aethalometer (AE33). Considered periods are the same as in Table 1.

		Whole event	PI	PII	PIII
	Site/Instruments				
BC_{ff}	SIRTA – AE33 ($PM_{2.5}$)	2.1	3.8	3.3	2.5
	Paris 13 –AE33 ($PM_{2.5}$)	3.6	9.1	4.3	2.9
BC_{wb}	SIRTA – AE33 ($PM_{2.5}$)	0.7	1.0	1.3	0.8
	Paris 13 – A33 ($PM_{2.5}$)	1.1	3.1	1.7	0.9
BC_{wb}/BC	SIRTA	26%	21%	28%	26%
	Paris 13	24%	25%	28%	23%

component during the episode. ISVOCs, whose gas-phase emissions are not part of EU directive on emission reduction yet, may largely contribute to OM. This is also in line with previous VOC source apportionment results obtained in the Paris region (Baudic et al., 2016; Languille et al., 2020). Primary ISVOCs may be emitted in both gas and particle phases by traffic and wood burning sources (Robinson et al., 2007; Kim et al., 2016) and can rapidly condense onto freshly emitted particles during cold winter time. Because a large fraction of ISVOCs condenses before undergoing oxidation, they are considered as primary compounds. In the simulations, particle-phase emissions of ISVOCs are taken into account in particle emissions (including OM emissions). Sensitivity simulations and tests with POLAIR3D/Polyphemus model show that simulated OM concentrations are very sensitive to the estimation of gas-phase ISVOC emissions. In the reference simulation, gas-phase ISVOC emissions are estimated by multiplying OM emissions by 1.5, as recommended in many studies (Bergström et al., 2012; Koo et al., 2014; Kim et al., 2016). With this reference simulation, simulated and measured OM (for PM_1) concentrations at SIRTA compare fairly well (not shown). However, simulated OM in PM_1 concentrations is underestimated if gas-phase ISVOC emissions are ignored over the Île-de-France region, and largely overestimated if they are multiplied by a factor of 4 (as in Couvidat et al., 2012) rather than 1.5, thus underlying the large influence of primary organic emissions.

3.3.2. *Inorganic components of PM: ammonium nitrate and ammonium sulfate*

Ammonium nitrate (NH_4NO_3) is another important component of PM pollution. At an annual scale, ammonia emissions from agricultural practices are maximum during spring, leading to high concentrations of ammonium nitrate (Petit et al., 2017; Fortems-Cheiney et al., 2020). Ammonia (NH_3) emissions from traffic may also lead to an increase in inorganic concentrations by up to 26% at traffic sites (Lugon et al., 2021). Enhanced ammonium nitrate concentrations can also be observed during winter, when ammonia emissions are smaller than during spring, because of the lower temperatures pushing gas – particle equilibria toward the particle phase. Enhanced NH_4NO_3 levels have been observed from ACSM measurements during the whole period with mean concentrations between 10 µg.m^{-3} at Gennevilliers (above 20% of the total PM1 fraction) and 5 µg.m^{-3} at SIRTA (27% of the total PM_1 fraction). Slightly higher values are observed at all sites (Table 3) during the PI and PII periods. As expected, filter observations at Creil and SIRTA of $PM_{2.5}$ fractions are consistent with PM_1 ACSM values. Such levels are consistent with the SIRTA phenomenology presented by Petit et al. (2015).

During the pollution event, weekly NH_3 measurements were performed in the Paris region in the framework of the NUAGE project (Personne et al., 2019). Table 5 shows a synthesis of these measurements. The largest amount of NH_3 is indeed observed during the "Spring" period ("March to May" in Table 5) while lowest values are observed between November and February. Highest values are consistently observed at the traffic site of BPEst. During "winter" (November to February) the BPEst site and the urban background station of Gennevilliers show clearly the highest NH_3 levels while values at rural sites remain lower thus highlighting likely the impact of the traffic source. During the three weeks of the pollution event, again a strong enhancement is observed at traffic and urban stations, with largest values during Week 2. Thus, gaseous NH_3 is still present during winter and there are indications that a traffic source is at least locally important (in addition to the major agricultural source) possibly leading to a rapid on-site formation of ammonium nitrate (Dall'Osto et al., 2009; Wang et al.,

Table 5
Mean weekly NH_3 concentrations (in ug.m^{-3}) performed with RADIELLO passive samplers at several sites in the IDF region conducted during the NUAGE project between 2016/07/04 and 2017/10/01. Week 1 is the week between 2016/11/28 and 2016/12/04. Week 2 is the week between 2016/12/05 and 2016/12/11. Week 3 is the week between 2016/12/12 and 2016/12/18.

	BP-Est (traffic)	Gennevilliers (Urban)	Rural-East	Rural-North	Rural-South
full period	4.9	3.1	2.3	2.0	2.5
Nov. to Feb.	3.8	1.8	0.8	0.9	1.5
March to May	6.1	4.1	3.8	3.5	4.9
Week 1 (W1)	4.7	1.9	0.8	0.8	0.5
Week 2 (W2)	6.3	3.9	0.9	1.6	0.6
Week 3 (W3)	5.1	2.6	0.8	0.9	0.6

2020).

In order to evaluate the relative impact of ammonia emissions on the formation of nitrate during the December 2016 period, we conducted sensitivity simulations with the CHIMERE model. According to emission inventories, more than 97% of ammonia emissions are associated to agricultural practices (only 85% for the Airparif emission inventory covering the IDF region). Following the EMEP inventory used as input data of the CHIMERE model, 94% of ammonia emissions over the IDF region are still associated with agriculture during December 2016 (in fact scaled on 2014 December emissions) even if fertilizer activities were likely reduced during this period. We simulated nitrate concentrations for specific sensitivity scenarios for NH_3 emissions (Fig. 13). If only agricultural emissions are considered, i.e. emissions from transport, industry and waste are removed, the part of nitrate explained by these "other" emissions can reach up to 25% for the most polluted (and probably local) part of the event (i.e. nitrate concentrations drop by up to 25% for this scenario especially in the Paris region). For the PII period, a contribution ranging from 15 to 20% can be reached within the plume and be attributed to emissions from other sources than agriculture. This is qualitatively well in line with NUAGE observations of NH_3 and the Airparif inventory (not used in our simulation) that illustrate the importance of the traffic source during winter. However, simulations are not meant to quantitatively predict the impact of traffic NH_3 emissions to nitrate, as the traffic emissions fraction in EMEP seems rather uncertain. This study illustrates that, local gradients for this nitrate fraction occur within the IDF region due to local emissions even if regional and rather homogeneous plumes generally dominate.

Concentrations of the sulfate (SO_4^{2-}) component, associated with industrial or ship emission sources, were low during this event (generally <2 µg.m^{-3}) and relatively constant between sites and periods (see Table 1) except in Creil. This can be explained by the local character of this episode (see below) combined to the low degree of industrialization of the Paris agglomeration.

3.3.3. *Oxidative potential*

The fine fraction of aerosols was found to be the main factor in the particle-induced pro-inflammatory response in Paris during the winter season. (Ramgolam et al., 2009). To complete this analysis of the December 2016 pollution event, we investigate in more detail the oxidative potential (OP) observations that were made during the event at the SIRTA and LISA UPEC sites, the first reported for the Paris region. Two acellular tests (AA and DTT) were processed according to Calas et al. (2017, 2018) and Weber et al. (2018, 2021). This measure is based on the capacity of particles to oxidise the pulmonary environment and induce oxidative stress. This measure can be considered as a proxy for their subsequent toxicity due to oxidative stress. Fig. 14 presents the time series of OP^v (volumetric OP in nmol.min^{-1}.m^{-3}) and OP^m

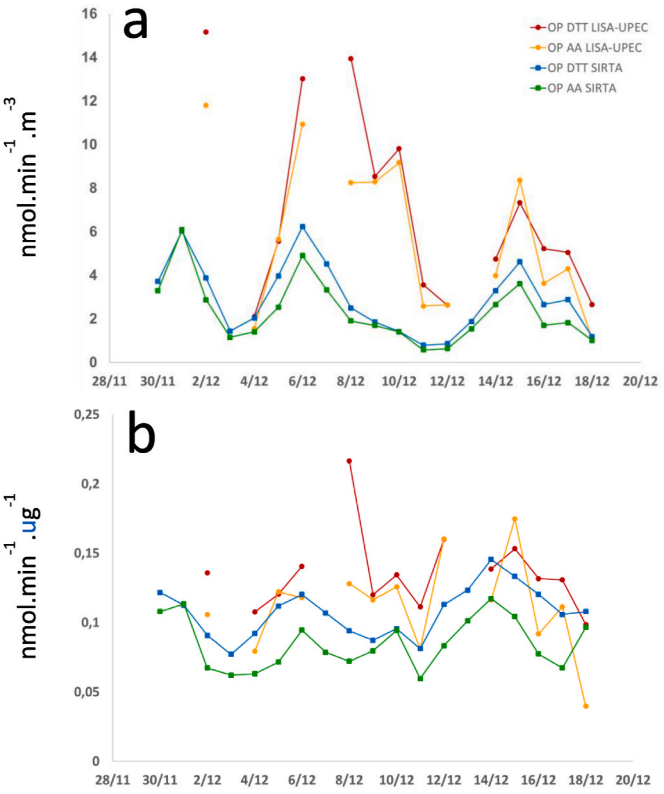

Fig. 14. Temporal series of (a) OP^v in nmol.min^{-1}.m^{-3} at LISA-UPEC and SIRTA for DTT and AA; (b) OP^m in nmol.min^{-1}.ug^{-1} at LISA-UPEC and SIRTA for DTT and AA.

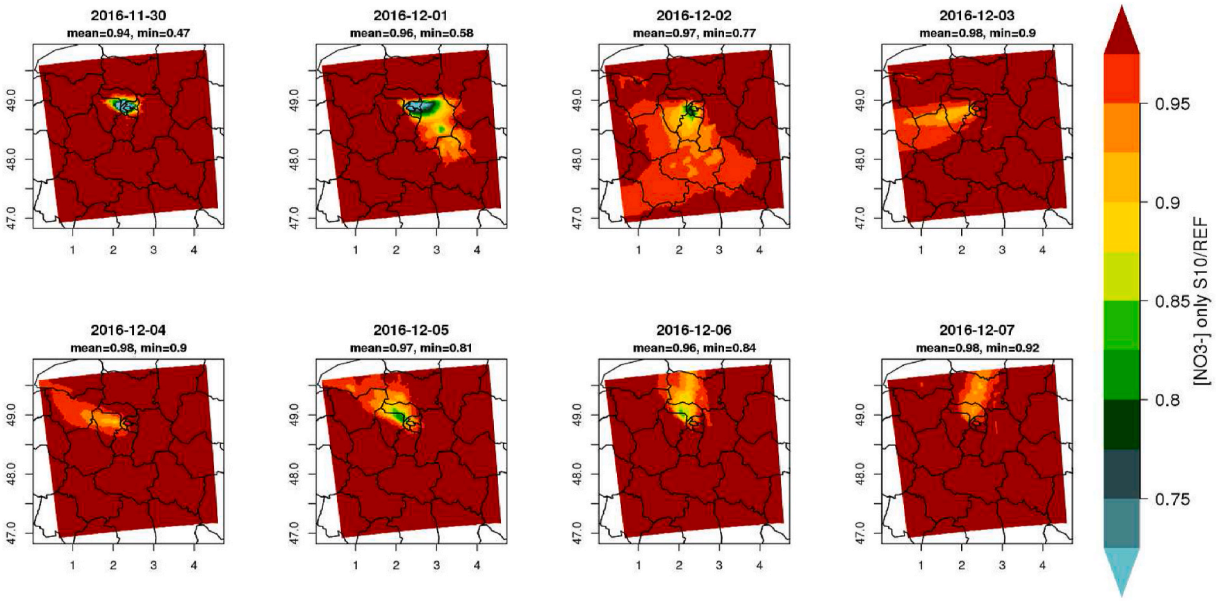

Fig. 13. Ratio of ammonium nitrate concentrations simulated by taking into account only NH_3 emissions from agricultural sector divided by nitrate concentrations from reference simulation. Simulations have been achieved using the CHIMERE model.

(intrinsic OP per ug of particle in nmol.min^{-1}.ug^{-1}) for AA and DTT during the event. It shows (Fig. 14a), for both tests, values of OP^{v} are in fair agreement with the dynamic of the PM mass concentrations. The maximum values observed at LISA-UPEC for this period are high compared to those usually observed in urban areas and comparable to those at roadside sites (Daellenbach et al., 2020; Weber et al., 2018). OP^{v} levels observed at SIRTA are lower because of lower aerosol concentrations and could be due to the different sampled fraction of PM (PM_{10} at Créteil and $PM_{2.5}$ at SIRTA) since PM_{10} may contains more metals associated to abrasion emissions (Grange et al., 2022). Looking at intrinsic OP^{m} (i.e. independent of PM concentrations) on Fig. 14b, we do see more similar values at both sites between 0.05 and 0.15 nmol min^{-1}. ug^{-1}, with slightly lower values at SIRTA. OP^{m} values above 0.15 nmol min^{-1}.ug^{-1} were observed during 4 days and they are rare among site typologies already published. Indeed, they often characterize a very dense urban environment as a traffic station or an industrial site (Barraza et al., 2020; Daellenbach et al., 2020). These high values highlight this intense pollution event as neither site is classified as industrial or traffic. Such values could also result from mixing/ageing of the aerosols that have enhanced their oxidative reactivity (Chowdhury, 2018). Nevertheless, such intrinsic OP values are close to traffic and biomass burning sources as shown by Weber et al. (2018) for several sites in France for both DTT and AA tests. This analysis could suggest an important implication of the strongly primary BC and OM-related character of this pollution event, which has particularly strong expected impacts on human health.

3.4. Analysis of the local versus advected contribution to PM

For control policies it is important to evaluate the origin of pollutants – especially for extreme events in December 2016. The nature of this pollution event is hence further discussed.

The meteorological situation that occurred in December 2016 (see Sub-section 2.2) is characterized by stagnant flow and, extremely low ventilation. This favors local accumulation of air pollutants and suggests local sources are of augmented importance. Both observations and numerical simulations highlight a mostly isotropic structure of concentration features for the IDF study area, especially during PI when ventilation is the weakest.

The very high levels of BC observed at Paris 13, Creil or LISA UPEC stations underline the dominance of local emission sources (Table 3) as BC is considered as a marker of local emissions. Further is OM found to be mostly of primary origin as underlined by Skyllakou et al. (2014) for the IDF. Moreover, the BC/SO_4^{2-} ratio at SIRTA and Creil sites reach values > 2 (Table 3) which illustrates the predominance of local sources associated to high BC levels as compared to remote sources outside the IDF characterized by larger relative fraction of sulfate concentrations and a BC/$SO4^{2-}$ ratio of 0.5 when advection dominates (Petit et al., 2015).

Finally, a sensitivity simulation was conducted using the POLAIR3D/Polyphemus model to estimate the impact of long-range transport on PM concentrations, by setting boundary conditions over the Île-de-France region to zero following the brute-force approach classically used for source apportionment (Belis et al., 2020). Comparisons of the reference and the sensitivity simulations (not shown) allow to estimate the contribution of local emissions and long-range transport on PM concentrations over the domain. Over Paris, about 89% of PM_{10} and $PM_{2.5}$ concentrations are due to local emissions (80% at the SIRTA site) for the considered period.

4. Conclusions and perspectives

This paper analyses the drivers of a severe pollution event that occurred over the Paris region in December 2016, taking advantage of multisite measurements of particulate matter, aerosol composition, oxidative potential and boundary layer dynamics.

The pollution event stands out, compared to proceeding ten years (2007–2017), both in terms of intensity and duration. Reduced total ventilation as a consequence of low horizontal transport (calm winds) coincides with very weak vertical mixing (very stable atmospheric stratification, shallow boundary layer heights) in a stagnant synoptic high-pressure circulation at the beginning of the pollution event. These dynamics leads to the highest PM_{10} levels observed at some of the Airparif monitoring stations within the past ten years, especially in the eastern part of the IDF close to Paris, where local pollution sources are intense. This suggests that the December 2016 event is mainly driven by local sources of pollution. A detailed characterization of atmospheric dynamics and their spatial variability is expected to provide further insights into the accumulation of air pollutants under such extreme conditions in the future.

The analysis of the PM chemical composition shows that OM highly dominates the total PM concentrations during this pollution episode. OM concentrations are higher for urban and traffic sites than at rural locations and the suburban SIRTA site. Combined with the fact that OM was mainly of primary origins, this is pointing again toward local sources, with predominant contributions from biomass burning (revealed as BBOA from PMF analysis from ACSM data at SIRTA). The relative amount of BC originating from wood burning compared to BC from fossil fuel combustion is about 20% during the event. This contribution is not very far from values classically observed during winter at SIRTA or even in Paris. Different numerical simulations confirm the predominance of local sources with about 80% explained by these sources. Simulations point out the strong contribution of primary intermediate and semi volatile organic compounds to OM. They are emitted by combustion processes from traffic and wood burning for residential heating. Their gas-phase emissions are not regulated yet, and a better characterization of those compounds is therefore necessary to limit OM concentrations during this type of pollution event. As common in IDF, ammonium nitrate is the second main component of the aerosol accumulation mode, even though agricultural emissions are less important during this season. NH_3 measurements show a significant traffic contribution to these relatively high values of ammonium nitrate. From model results it is estimated that up to 25% of ammonium nitrate are related to ammonia emissions of traffic, waste or industry sectors within the Paris region. The predominance of local sources in very stable meteorological conditions can lead to strong spatial gradients within the urban area as illustrated by both network observations and numerical simulations.

The integrated methodology developed for the present study based on a network of observational sites as well as specific model simulations is proven valuable for the investigation of pollution episodes and for the quantification of local against remote origins at the regional scale, which is of prime interest for emission control policies. In future studies, we will also focus more on the health impact of PM pollution, according to their chemical composition.

The analysis of the oxidative potential of PM during this pollution event adds valuable estimates of the possible health impacts associated to the local urban emissions observed. The oxidative potential measurements during the pollution event indicate that the PM mass-weighted oxidative potential values are significant and consistent with the predominant primary sources of traffic and biomass burning This opens an important perspective, which deserves further analysis for a wide range of observations: in addition to the high PM mass concentrations during this outstanding (for the Paris area) low dispersion pollution event, the observed large mass specific OP values even raise concerns for a more significant health impact.

CRediT authorship contribution statement

G. Foret: Conceptualization, Writing – review & editing. **V. Michoud:** Conceptualization, Writing – review & editing. **S. Kotthaus:** Conceptualization, Writing – review & editing. **J.-E. Petit:**

Conceptualization, Data curation, Writing – review & editing. **A. Baudic:** Conceptualization, Resources, Data curation, Writing – review & editing. **G. Siour:** Conceptualization, Software, Writing – review & editing. **Y. Kim:** Software. **J.-F. Doussin:** Conceptualization, Writing – review & editing. **J.-C. Dupont:** Resources, Data curation. **P. Formenti:** Data curation, Writing – review & editing. **C. Gaimoz:** Resources, Data curation. **V. Ghersi:** Conceptualization, Resources, Data curation. **A. Gratien:** Conceptualization, Writing – review & editing. **V. Gros:** Conceptualization, Writing – review & editing. **J.-L. Jaffrezo:** Conceptualization, Writing – review & editing. **M. Haeffelin:** Conceptualization, Writing – review & editing. **M. Kreitz:** Conceptualization, Writing – review & editing. **F. Ravetta:** Conceptualization, Writing – review & editing. **K. Sartelet:** Conceptualization, Writing – review & editing. **L. Simon:** Formal analysis. **Y. Té:** Conceptualization, Resources, Data curation, Writing – review & editing. **G. Uzu:** Conceptualization, Writing – review & editing. **S. Zhang:** Resources, Data curation. **O. Favez:** Conceptualization, Resources, Data curation, Writing – review & editing. **M. Beekmann:** Conceptualization, Writing – review & editing.

Declaration of competing interest

The authors declare that they have no known competing financial interests or personal relationships that could have appeared to influence the work reported in this paper.

Data availability

Data will be made available on request.

Acknowledgments

Measurements at SIRTA have been supported by CNRS, CEA, INERIS; Ile de France region and ACTRIS-France (notably through the CLAP national observation service). They were also part of the EUFP7 and H2020 ACTRIS projects (grant agreements Nos. 262254 and 654109). Measurements and analyses carried out at the LISA UPEC station were supported by L. Beillard, S. Chevaillier, A. Féron, A.-C. Guillet M. Maillé, F. Maisonneuve, C. Mirande-Bret, S. Triquet. This work was performed using HPC resources from GENCI-IDRIS (Grant 2020-A0090107232) The authors would also like to thank both Erwan Personne (INRA) for the coordination of the NUAGE research project and the ADEME (French Agency for Environmental and Energy Management) for its financial support through the CORTEA program. We are grateful to Sorbonne Université and Institut Pierre-Simon Laplace for support and facilities, as well as Pascal Jeseck for the CO11M measurement support. This work has been funded by the French CNRS LEFE-CHAT program in the framework of the EPPI project. JLJ and GU thank ANR10 LABX56 and ANR-15-IDEX-02 for funding instruments in Air-O-Sol facility.

Appendix A. Supplementary data

Supplementary data to this article can be found online at https://doi.org/10.1016/j.atmosenv.2022.119386.

References

Aïchi, L., Husson, J.-P., 2015. « Pollution de l'air : le coût de l'inaction », Rapport de la commission d'enquête du Sénat sur le coût économique et financier de la pollution de l'air, rapport du sénat, p. 610. http://www.senat.fr/rap/r14-610-1/r14-610-11.pdf.

Aiken, A.C., DeCarlo, P.F., Kroll, J.H., Worsnop, D.R., Huffman, J.A., Docherty, K.S., Ulbrich, I.M., Mohr, C., Kimmel, J.R., Sueper, D., et al., 2008. O/C and OM/OC ratios of primary, secondary, and ambient organic aerosols with high-resolution time-of-flight aerosol mass spectrometry. Environ. Sci. Technol. 42, 4478–4485.

Airparif, 2017. Bilan de la qualité de l'air –2016 – Surveillance et information en Île-de-France. Juin.

Airparif, 2020. Bilan de la qualité de l'air –2019 – Surveillance et information en Île-de-France. Juin.

Ait-Helal, W., Borbon, A., Sauvage, S., de Gouw, J.A., Colomb, A., Gros, V., Freutel, F., Crippa, M., Afif, C., Baltensperger, U., Beekmann, M., Doussin, J.-F., Durand-Jolibois, R., Fronval, I., Grand, N., Leonardis, T., Lopez, M., Michoud, V., Miet, K., Perrier, S., Prévôt, A.S.H., Schneider, J., Siour, G., Zapf, P., Locoge, N., 2014. Volatile and intermediate volatility organic compounds in suburban Paris: variability, origin and importance for SOA formation. Atmos. Chem. Phys. 14, 10439–10464. https://doi.org/10.5194/acp-14-10439-2014.

Barraza, F., Uzu, G., Jaffrezo, J.-L., Schreck, E., Budzinski, H., Le Menach, K., Dévier, M.-H., Guyard, H., Calas, A., Perez, M.-I., Villacreces, L.-A., Maurice, L., 2020. Contrasts in chemical composition and oxidative potential in PM10 near flares in oil extraction and refining areas in Ecuador. Atmos. Environ. 223.

Bates, J.T., Weber, R.J., Verma, V., Fang, T., Ivey, C., Liu, C., Sarnat, S.E., Chang, H.H., Mulholland, J.A., Russell, A., 2018. Source impact modeling of spatiotemporal trends in PM2.5 oxidative potential across the eastern United States. Atmos. Environ. 193, 158–167.

Baudic, A., Gros, V., Sauvage, S., Locoge, N., Sanchez, O., Sarda-Estève, R., Kalogridis, C., Petit, J.E., Bonnaire, N., Baisnée, D., Favez, O., Albinet, A., Sciare, J., Bonsang, B., 2016. Seasonal variability and source apportionment of volatile organic compounds (VOCs) in the Paris megacity (France). Atmos. Chem. Phys. 16, 11961–11989. https://doi.org/10.5194/acp-16-11961-2016.

Beekmann, M., Prévôt, A.S.H., Drewnick, F., Sciare, J., Pandis, S.N., Denier van der Gon, H.A.C., Crippa, M., Freutel, F., Poulain, L., Ghersi, V., Rodriguez, E., Beirle, S., Zotter, P., von der Weiden-Reinmüller, S.-L., Bressi, M., Fountoukis, C., Petetin, H., Szidat, S., Schneider, J., Rosso, A., El Haddad, I., Megaritis, A., Zhang, Q.J., Michoud, V., Slowik, J.G., Moukhtar, S., Kolmonen, P., Stohl, A., Eckhardt, S., Borbon, A., Gros, V., Marchand, N., Jaffrezo, J.L., Schwarzenboeck, A., Colomb, A., Wiedensohler, A., Borrmann, S., Lawrence, M., Baklanov, A., Baltensperger, U., 2015. In situ, satellite measurement and model evidence on the dominant regional contribution to fine particulate matter levels in the Paris megacity. Atmos. Chem. Phys. 15, 9577–9591. https://doi.org/10.5194/acp-15-9577-2015.

Belis, C.A., Pernigotti, D., Pirovano, G., Favez, O., Jaffrezo, J.L., Kuenen, J., Denier van Der Gon, H., Reizer, M., Riffault, V., Alleman, L.Y., Almeida, M., Amato, F., Angyal, A., Argyropoulos, G., Bande, S., Beslic, I., Besombes, J.-L., Bove, M.C., Brotto, P., Calori, G., Cesari, D., Colombi, C., Contini, D., De Gennaro, G., Di Gilio, A., Diapouli, E., El Haddad, I., Elbern, H., Eleftheriadis, K., Ferreira, J., Garcia Vivanco, M., Gilardoni, S., Golly, B., Hellebust, S., Hopke, P.K., Izadmanesh, Y., Jorquera, H., Krajsek, K., Kranenburg, R., Lazzeri, P., Lenartz, F., Lucarelli, F., Maciejewska, K., Manders, A., Manousakas, M., Masiol, M., Mircea, M., Mooibroek, D., Nava, S., Oliveira, D., Paglione, M., Pandolfi, M., Perrone, M., Petralia, E., Pietrodangelo, A., Pillon, S., Pokorna, P., Prati, P., Salameh, D., Samara, C., Samek, L., Saraga, D., Sauvage, S., Schaap, M., Scotto, F., Sega, K., Siour, G., Tauler, R., Valli, G., Vecchi, R., Venturini, E., Vestenius, M., Waked, A., Yubero, E., 2020. Evaluation of receptor and chemical transport models for PM10 source apportionment. Atmos. Environ. 5.

Bergström, R., Denier van der Gon, H., Prévôt, A., Yttri, K., Simpson, D., 2012. Modelling of organic aerosols over Europe (2002-2007) using a volatility basis set (VBS) framework: application of different assumptions regarding the formation of secondary organic aerosol. Atmos. Chem. Phys. 12, 8499–8527.

Calas, A., Uzu, G., Martins, J.M.F., Voisin, D., Spadini, L., Lacroix, T., Jaffrezo, J.L., 2017. The importance of simulated lung fluid (SLF) extractions for a more relevant evaluation of the oxidative potential of particulate matter. Sci. Rep.-UK 7, 11617. https://doi.org/10.1038/s41598-017-11979-3.

Calas, A., Uzu, G., Kelly, F.J., Houdier, S., Martins, J.M.F., Thomas, F., Molton, F., Charron, A., Dunster, C., Oliete, A., Jacob, V., Besombes, J.-L., Chevrier, F., Jaffrezo, J.-L., 2018. Comparison between five acellular oxidative potential measurement assays performed with detailed chemistry on PM10 samples from the city of Chamonix (France). Atmos. Chem. Phys. 18, 7863–7875. https://doi.org/10.5194/acp-18-7863-2018.

Canonaco, F., Crippa, M., Slowik, J.G., Baltensperger, U., Prévôt, A.S.H., 2013. SoFi, an IGORbased interface for the efficient use of the generalized multilinear engine (ME-2) for the source apportionment: ME-2 application to aerosol mass spectrometer data. Atmos. Meas. Tech. 6, 3649–3661.

Charrier, J.G., Anastasio, C., 2012. On dithiothreitol (DTT) as a measure of oxidative potential for ambient particles: evidence for the importance of soluble transition metals. Atmos. Chem. Phys. 12, 9321–9333. https://doi.org/10.5194/acp-12-9321-2012.

Choi, Y.J., Kim, S.H., Kang, S.H., et al., 2019. Short-term effects of air pollution on blood pressure. Sci. Rep. 9 https://doi.org/10.1038/s41598-019-56413-y, 20298.

Chowdhury, Pratiti Home, et al., 2018. Exposure of lung epithelial cells to photochemically aged secondary organic aerosol shows increased toxic effects. Environ. Sci. Technol. Lett. 424–430.

Cholakian, A., Beekmann, M., Colette, A., Coll, I., Siour, G., Sciare, J., et al., 2018. Simulation of fine organic aerosols in the western Mediterranean area during the ChArMEx 2013 summer campaign. Atmos. Chem. Phys. 18 (10), 7287–7312.

Chrit, M., Sartelet, K., Sciare, J., Majdi, M., Nicolas, J., Petit, J.-E., Dulac, F., 2018. Modeling organic aerosol concentrations and properties during winter 2014 in the northwestern Mediterranean region. Atmos. Chem. Phys. 18, 18079–18100. https://doi.org/10.5194/acp-18-18079-2018.

Cohen, A.J., Brauer, M., Burnett, R., Anderson, H.R., Frostad, J., Estep, K., Balakrishnan, K., Brunekreef, B., Dandona, L., Dandona, R., Feigin, V., Freedman, G., Hubbell, B., Jobling, A., Kan, H., Knibbs, L., Liu, Y., Martin, R., Morawska, L., Pope, C.A., Shin, H., Straif, K., Shaddick, G., Thomas, M., van Dingenen, R., van Donkelaar, A., Vos, T., Murray, C.J.L., Forouzanfar, M.H., 2017. Estimates and 25-year trends of the global burden of disease attributable to ambient air pollution: an analysis of data from the Global Burden of Diseases Study. Lancet 389 (10082), 1907–1918, 2017.

Couvidat, F., Debry, E., Sartelet, K., Seigneur, C., 2012. A hydrophilic/hydrophobic organic (H^2O) model: model development, evaluation and sensitivity analysis. J. Geophys. Res. 117, D10304 https://doi.org/10.1029/2011JD017214.

Couvidat, F., Kim, Y., Sartelet, K., Seigneur, C., Marchand, N., Sciare, J., 2013. Modeling secondary organic aerosol in an urban area: application to Paris. France. Atmos. Chem. Phys. 13, 983–996.

Couvidat, F., Sartelet, K., 2015. The Secondary Organic Aerosol Processor (SOAP v1. 0) model: a unified model with different ranges of complexity based on the molecular surrogate approach. Geosci. Model Dev. (GMD) 8 (4), 1111–1138.

Daellenbach, K.R., Uzu, G., Jiang, J., et al., 2020. Sources of particulate-matter air pollution and its oxidative potential in Europe. Nature 587, 414–419. https://doi.org/10.1038/s41586-020-2902-8.

Dall'Osto, M., Harrison, R.M., Coe, H., Williams, P.I., Allan, J.D., 2009. Real time chemical characterization of local and regional nitrate aerosols. Atmos. Chem. Phys. 9, 3709–3720. https://doi.org/10.5194/acp-9-3709-2009.

Debry, E., Fahey, K., Sartelet, K., Sportisse, B., Tombette, M., 2007. A new SIze REsolved aerosol model (SIREAM). Atmos. Chem. Phys. 7 (6), 1537–1547.

Emmons, L.K., Walters, S., Hess, P.G., Lamarque, J.-F., Pfister, G.G., Fillmore, D., Granier, C., Guenther, A., Kinnison, D., Laepple, T., Orlando, J., Tie, X., Tyndall, G., Wiedinmyer, C., Baughcum, S.L., Kloster, S., 2010. Description and evaluation of the model for ozone and related chemical tracers, version 4 (MOZART-4), geosci. Model Dev 3, 43–67. https://doi.org/10.5194/gmd-3-43-2010.

El Haddad, I., Marchand, N., Dron, J., Temime-Roussel, B., Quivet, E., Wortham, H., Jaffrezo, J.L., Baduel, C., Voisin, D., Besombes, J.L., et al., 2009. Comprehensive primary particulate organic characterization of vehicular exhaust emissions in France. Atmos. Environ. 43, 6190–6198.

EU, 2008. Directive 2008/50/EC of the European Parliament and of the cCouncil of 21 May 2008 on Ambient Air Quality and Cleaner Air for Europe.

Favez, O., Cachier, H., Sciare, J., Le Moullec, Y., 2007. Characterization and contribution to PM2.5 of semi-volatile aerosols in Paris (France). Atmos. Environ. 41, 7969–7976.

Favez, O., Cachier, H., Sciare, J., Sarda-Estève, R., Martinon, L., 2009. Evidences for a significant contribution of wood burning aerosols to $PM_{2.5}$ during the winter season in Paris, France. Atmos. Environ. 43, 3640–3644.

Favez, O., Weber, S., Petit, J.-E., Alleman, L.Y., Albinet, A., Riffault, V., Chazeau, B., Amodeo, T., Salameh, D., Zhang, Y., Srivastava, D., Samaké, A., Aujay-Plouzeau, R., Papin, A., Bonnaire, N., Boullanger, C., Chatain, M., Chevrier, F., Detournay, A., Dominik-Sègue, M., Falhun, R., Garbin, C., Ghersi, V., Grignion, G., Levigoureux, G., Pontet, S., Rangognio, J., Zhang, S., Besombes, J.-L., Conil, S., Uzu, G., Savarino, J., Marchand, N., Gros, V., Marchand, C., Jaffrezo, J.-L., Leoz-Garziandia, E., 2021. Overview of the French operational network for in situ observation of PM chemical composition and sources in urban environments (CARA program). Atmosphere 12 (2), 207. https://doi.org/10.3390/atmos12020207.

Fortems-Cheiney, A., Foret, G., Siour, G., Vautard, R., Szopa, S., Dufour, G., Colette, A., Lacressonniere, Gwendoline, Beekmann, M., 2017. A 3°C global RCP8.5 emission trajectory cancels benefits of European emission reductions on air quality. Nat. Commun. 8 (89).

Fortems-Cheiney, A., Dufour, G., Dufossé, K., Couvidat, F., Gilliot, J.-M., Siour, G., Beekmann, M., Foret, G., Meleux, F., Clarisse, L., Coheur, P.-F., Van Damme, M., Clerbaux, C., Génermont, 2020. Do alternative inventories converge on the spatiotemporal representation of spring ammonia emissions in France. Atmos. Chem. Phys. 20, 13481–13495.

Giani, P., Balzarini, A., Pirovano, G., Gilardoni, S., Paglione, M., Colombi, C., Gianelle, V. L., Belis, C.A., Poluzzi, V., Lonati, G., 2019. Influence of semi- and intermediate-volatile organic compounds (S/IVOC) parameterizations, volatility distributions and aging schemes on organic aerosol modelling in winter conditions. Atmos. Environ. 213, 11–24. https://doi.org/10.1016/j.atmosenv.2019.05.061.

Ginoux, P., Chin, M., Tegen, I., Prospero, J.M., Holben, B., Dubovik, O., Lin, S.J., 2001. Sources and distributions of dust aerosols simulated with the GOCART model. J. Geophys. Res. Atmos. 106 (D17), 20255–20273.

Grange, S.K., Uzu, G., Weber, S., Jaffrezo, J.-L., Hueglin, C., 2022. Linking Switzerland's PM10 and PM2.5 oxidative potential (OP) with emission sources. Atmos. Chem. Phys. 22, 7029–7050. https://doi.org/10.5194/acp-22-7029-2022.

Guenther, A., Karl, T., Harley, P., Wiedinmyer, C., Palmer, P.I., Geron, C., 2006. Estimates of global terrestrial isoprene emissions using MEGAN (model of emissions of Gases and aerosols from nature). Atmos. Chem. Phys. 6, 3181–3210. https://doi.org/10.5194/acp-6-3181-2006.

Hauglustaine, D.A., Balkanski, Y., Schulz, M., 2014. A global model simulation of present and future nitrate aerosols and their direct radiative forcing of climate. Atmos. Chem. Phys. 14 (20), 11031–11063.

Hersbach, H., Bell, B., Berrisford, P., et al., 2020. The ERA5 global reanalysis. Q. J. R. Meteorol. Soc. 146, 1999–2049. https://doi.org/10.1002/qj.3803.

Horton, D.E., Skinner, C.B., Singh, D., Diffenbaugh, N.S., 2014. Occurrence and persistence of future atmospheric stagnation events. Nat. Clim. Change 4, 698–703. https://doi.org/10.1038/nclimate2272.

Hou, P., Wu, S., 2016. Long-term changes in extreme air pollution meteorology and the implications for air quality. Sci. Rep. 6, 23792 https://doi.org/10.1038/srep23792.

Kalnay, et al., 1996. The NCEP/NCAR 40-year reanalysis project. Bull. Am. Meteorol. Soc. 77, 437–470.

Katsouyanni, K., Samet, J.M., Anderson, H.R., et al., 2009. Air Pollution and Health: a European and North American Approach (APHENA), Research Report, vol. 142. Health Effects Institute), pp. 5–90.

Katsouyanni, K., Schwartz, J., Spix, C., Touloumi, G., Zmirou, D., Zanobetti, A., Wojtyniak, B., Vonk, J.M., Tobias, A., Pönkä, A., Medina, S., Bachárová, L., Anderson, H.R., 1996. Short term effects of air pollution on health: a European approach using epidemiologic time series data: the APHEA protocol. J. Epidemiol. Community Health 50 (Suppl. 1), S12–S18. https://doi.org/10.1136/jech.50.suppl_1.s12. PMID: 8758218; PMCID: PMC1060882.

Kim, Y., Sartelet, K., Seigneur, C., 2011. Formation of secondary aerosols over Europe: comparison of two gas-phase chemical mechanisms. Atmos. Chem. Phys. 11 (2), 583–598.

Kim, Y., Sartelet, K., Raut, J.-C., Chazette, P., 2015. Influence of an urban canopy model and PBL schemes on vertical mixing for air quality modeling over Greater Paris. Atmos. Environ. 107, 289–306.

Kim, Y., Sartelet, K., Seigneur, C., Charron, A., Besombes, J.-L., Jaffrezo, J.-L., Marchand, N., Polo, L., 2016. Effect of measurement protocol on organic aerosol measurements of exhaust emissions from gasoline and diesel vehicles. Atmos. Environ. 140, 176–187.

Koo, B., Knipping, E., Yarwood, G., 2014. 1.5- Dimensional volatility basis set approach for modeling organic aerosol in CAMx and CMAQ. Atmos. Environ. 95, 158–164.

Kotthaus, S., Grimmond, S., 2018. Atmospheric boundary layer characteristics from ceilometer measurements Part 1: a new method to track mixed layer height and classify clouds. Q. J. R. M. S. 144, 1525–1538. https://rmets.onlinelibrary.wiley.com/doi/full/10.1002/qj.3299.

Kotthaus, S., Haeffelin, M., Drouin, M.A., Dupont, J.C., Grimmond, S., Haefele, A., Hervo, M., Poltera, Y., Wiegner, M., 2020. Tailored algorithms for the detection of the atmospheric boundary layer height from common automatic lidars and ceilometers (ALC). Rem. Sens. 12, 3259. https://www.mdpi.com/2072-4292/12/19/3259.

Languille, B., Gros, V., Petit, J.-E., Honoré, C., Baudic, A., Perrussel, O., Foret, G., Michoud, V., Truong, F., Bonnaire, N., Sarda-Estève, R., Delmotte, M., Feron, A., Maisonneuve, F., Gaimoz, C., Formenti, P., Kotthaus, S., Haeffelin, M., Favez, O., 2020. Wood burning: a major source of Volatile Organic Compounds during wintertime in the Paris region. Sci. Total Environ. 711, 135055 https://doi.org/10.1016/j.scitotenv.2019.135055.

LCSQA, 2015. Impact de la Combustion de Biomasse sur les Concentrations de PM10 (Programme CARA—Hiver 2014–2015) online: https://www.lcsqa.org/fr/rapport/2015/ineris/impact-combustion-biomasse-concentrationspm10-programme-carahiver- 2014-2015. (Accessed 24 August 2021).

Leni, Z., Cassagnes, L.-E., Daellenbach, K.R., El Haddad, I., Vlachou, A., Uzu, G., Prévôt, A.S.H., Jaffrezo, J.-L., Baumlin, N., Salathe, M., Baltensperger, U., Dommen, J., Geiser, M., 2020. Oxidative stress-induced inflammation in susceptible airways by anthropogenic aerosol. PLoS One 18. https://doi.org/10.1371/journal.pone.0233425.

Lugon, L., Sartelet, K., Kim, Y., Vigneron, J., Chrétien, O., 2021. Simulation of primary and secondary particles in the streets of Paris using MUNICH. Faraday Discuss 226, 432–456. https://doi.org/10.1039/D0FD00092B.

Marécal, V., Peuch, V.-H., Andersson, C., Andersson, S., Arteta, J., Beekmann, M., Benedictow, A., Bergström, R., Bessagnet, B., Cansado, A., Chéroux, F., Colette, A., Coman, A., Curier, R.L., Denier van der Gon, H.A.C., Drouin, A., Elbern, H., Emili, E., Engelen, R.J., Eskes, H.J., Foret, G., Friese, E., Gauss, M., Giannaros, C., Guth, J., Joly, M., Jaumouillé, E., Josse, B., Kadygrov, N., Kaiser, J.W., Krajsek, K., Kuenen, J., Kumar, U., Liora, N., Lopez, E., Malherbe, L., Martinez, I., Melas, D., Meleux, F., Menut, L., Moinat, P., Morales, T., Parmentier, J., Piacentini, A., Plu, M., Poupkou, A., Queguiner, S., Robertson, L., Rouïl, L., Schaap, M., Segers, A., Sofiev, M., Tarasson, L., Thomas, M., Timmermans, R., Valdebenito, Á., van Velthoven, P., van Versendaal, R., Vira, J., Ung, A., 2015. A regional air quality forecasting system over Europe: the MACC-II daily ensemble production, Geosci. Model Dev 8, 2777–2813. https://doi.org/10.5194/gmd-8-2777-2015.

Medina, S., Adélaïde, L., Wagner, V., de Crouy Chanel, P., Real, E., Colette, A., Couvidat, F., et al., 2021. Impact de pollution de l'air ambiant sur la mortalité en France métropolitaine. Réduction en lien avec le confinement du printemps 2020 et nouvelles données sur le poids total pour la période 2016-2019. Saint-Maurice. Santé publique France, p. 63. www.santepubliquefrance.fr.

Michoud, V., Colomb, A., Borbon, A., Miet, K., Beekmann, M., Camredon, M., Aumont, B., Perrier, S., Zapf, P., Siour, G., Ait-Helal, W., Afif, C., Kukui, A., Furger, M., Dupont, J.C., Haeffelin, M., Doussin, J.F., 2014. Study of the unknown HONO daytime source at a European suburban site during the MEGAPOLI summer and winter field campaigns. Atmos. Chem. Phys. 14, 2805–2822. https://doi.org/10.5194/acp-14-2805-2014.

Murphy, B., Donahue, N., Robinson, A., Pandis, S., 2014. A naming convention for atmospheric organic aerosol Atmos. Chem. Phys. 14, 5825–5839. https://doi.org/10.5194/acp-14-5825-2014.

Paatero, P., Tapper, U., 1994. Positive matrix factorization: a non-negative factor model with optimal utilization of error estimates of data values. Environmetrics 5, 111–126. https://doi.org/10.1002/env.3170050203.

Pailleux, J., Geleyn, J.-F., Hamrud, M., Courtier, P., Thépaut, J.-N., Rabier, F., Andersson, E., Burridge, D., Simmons, A., Salmond, D., El Khatib, R., Fischer, C., 2014. Twenty-five years of IFS/Arpege. ECMWF Newsletter 141, 22–30.

Personne, E., Abbou, G., Joly, L., Sanchez, O., Cousin, J., Decarpentrie, T., Decuq, C., Dumelin, N., Esnault, B., Fortineau, A., Gueudet, J.-C., 2019. Développement de nouveaux dispositifs de mesures pour les émissions d'ammoniac dans l'air en région parisienne – NUAGE : Test des NoUveaux dispositifs pour mieux évaluer les flux d'Ammoniac dans l'atmosphère depuis les aGrosystèmes et Ecosystèmes et interprétation de la campagne de mesures à l'échelle de la région Île-de-France. Rapport, 106 pages. ADEME.

Petetin, H., Beekmann, M., Sciare, J., Bressi, M., Rosso, A., Sanchez, O., Ghersi, V., 2014. A novel model evaluation approach focusing on local and advected contributions to urban $PM_{2.5}$ levels – application to Paris. France, Geosci. Model Dev. 7, 1483–1505. https://doi.org/10.5194/gmd-7-1483-2014.

Petit, J.-E., Favez, O., Sciare, J., Canonaco, F., Croteau, P., Močnik, G., Jayne, J., Worsnop, D., Leoz-Garziandia, E., 2014. Submicron aerosol source apportionment of wintertime pollution in Paris, France by double positive matrix factorization (PMF^2) using an aerosol chemical speciation monitor. ACSM) and a multi-wavelength Aethalometer 14, 13773–13787. https://doi.org/10.5194/acp-14-13773-2014.

Petit, J.-E., Favez, O., Sciare, J., Crenn, V., Sarda-Estève, R., Bonnaire, N., Močnik, G., Dupont, J.-C., Haeffelin, M., Leoz-Garziandia, E., 2015. Two years of near real-time chemical composition of submicron aerosols in the region of Paris using an Aerosol Chemical Speciation Monitor. ACSM) and a multi-wavelength Aethalometer 15, 2985–3005, 670. https://doi.org/10.5194/acp-15-2985-2015.

Petit, J.-E., Amodeo, T., Meleux, F., Bessagnet, B., Menut, L., Grenier, D., Pellan, Y., Ockler, A., Rocq, B., Gros, V., Sciare, J., Favez, O., 2017. Characterising an intense PM pollution episode in March 2015 in France from multi-site approach and near real time data: climatology, variabilities, geographical origins and model evaluation. Atmos. Environ. 155, 68–84. https://doi.org/10.1016/j.atmosenv.2017.02.012.

Ramgolam, K., Favez, O., Cachier, H., Gaudichet, A., Marano, F., Martinon, L., Baeza-Squiban, A., 2009. Size-partitioning of an urban aerosol to identify particle determinants involved in the proinflammatory response induced in airway epithelial cells. Part. Fibre Toxicol. 6, 10. https://doi.org/10.1186/1743-8977-6-10.

Robinson, A., Donahue, N., Shrivastava, M., Weitkamp, E., Sage, A., Grieshop, A., Lane, T., Pierce, J., Pandis, S., 2007. Rethinking organic aerosols: semivolatile emissions and photochemical aging. Science 315, 1259–1262.

Rouil, L., Honoré, C., Vautard, R., Beekmann, M., Bessagnet, B., Malherbe, L., Meleux, F., Dufour, A., Elichegaray, C., Flaud, J.-M., Menut, L., Martin, D., Peuch, A., Peuch, V.-H., Poisson, N., 2009. PREV'AIR: an operational forecasting and mapping system for air quality in Europe. BAMS. https://doi.org/10.1175/2008BAMS2390.1.

Royer, P., Chazette, P., Sartelet, K., Zhang, Q.J., Beekmann, M., Raut, J.-C., 2011. Comparison of lidar-derived PM10 with regional modeling and ground-based observations in the frame of MEGAPOLI experiment. Atmos. Chem. Phys. 11, 10705–10726, 105194/acp-11-10705-2011.

Sartelet, K., Zhu, S., Moukhtar, S., André, M., André, J.M., Gros, V., Favez, O., Brasseur, A., Redaelli, M., 2018. Emission of intermediate, semi and low volatile organic compounds from traffic and their impact on secondary organic aerosol concentrations over Greater Paris. Atmos. Environ. 180, 126–137.

Sauvain, J.J., Setyan, A., Wild, P., et al., 2011. Biomarkers of oxidative stress and its association with the urinary reducing capacity in bus maintenance workers. J. Occup. Med. Toxicol. 6 (1–13).

Scheers, H., Nawrot, T.S., Nemery, B., et al., 2018. Changing places to study short-term effects of air pollution on cardiovascular health: a panel study. Environ. Health 17, 80. https://doi.org/10.1186/s12940-018-0425-7.

Sciare, J., d'Argouges, O., Zhang, Q.J., Sarda-Estève, R., Gaimoz, C., Gros, V., Beekmann, M., Sanchez, O., 2010. Comparison between simulated and observed chemical composition of fine aerosols in Paris (France) during springtime: contribution of regional versus continental emissions. Atmos. Chem. Phys. 10, 11987–12004. https://doi.org/10.5194/acp-10-11987-2010.

Shehab, M.A., Pope, F.D., 2019. Effects of short-term exposure to particulate matter air pollution on cognitive performance. Sci. Rep. 9, 8237. https://doi.org/10.1038/s41598-019-44561-0.

Shiraiwa, M., Ueda, K., Pozzer, A., Lammel, G., Kampf, C.J., Fushimi, A., Enami, S., Arangio, A.M., Fröhlich-Nowoisky, J., Fujitani, Y., Furuyama, A., Lakey, P.S.J., Lelieveld, J., Lucas, K., Morino, Y., Pöschl, U., Takahama, S., Takami, A., Tong, H., Weber, B., Yoshino, A., Sato, K., 2017. Environ. Sci. Technol. 51 (23), 13545–13567. https://doi.org/10.1021/acs.est.7b04417.

Skamarock, W.C., Klemp, J.B., Dudhia, J., Gill, D.O., Barker, D.M., Duda, M.G., Huang, X.-Y., Wang, W., Powers, J.G., 2008. A description of the Advanced Research WRF version 3. NCAR Tech. Note NCAR/TN-475+STR 113. https://doi.org/10.5065/D68S4MVH.

Skyllakou, K., Murphy, B.N., Megaritis, A.G., Fountoukis, C., Pandis, S.N., 2014. Contributions of local and regional sources to fine PM in the megacity of Paris. Atmos. Chem. Phys. 14, 2343–2352. https://doi.org/10.5194/acp-14-2343-2014.

Uzu, G., Sauvain, J.-J., Baeza-Squiban, A., Riediker, M., Sánchez Sandoval Hohl, M., Val, S., Tack, K., Denys, S., Pradère, P., Dumat, C., 2011. Environ. Sci. Technol. 45 (18), 7888–7895. https://doi.org/10.1021/es200374c.

Vautard, R., Colette, A., van Meijgaard, E., Meleux, F., van Oldenborgh, G.J., Otto, F., Tobin, I., Yiou, P., 2018. Attribution of wintertime anticyclonic stagnation contributing to air pollution in western Europe, [in "Explaining Extreme Events of 2016 from a Climate Perspective"]. Bull. Am. Meteorol. Soc. 99 (1), S54–S59. https://doi.org/10.1175/BAMS-D-17-0118.1.

Vestreng, V., 2003. Review and Revision, Emission Data Reported to CLRTAP Tech. Rep., EMEP MSW-W, Tech. Rep. Norwegian Meteorological Institute, Oslo, Norway.

Wang, Y., Sartelet, K., Bocquet, M., Chazette, P., 2014. Modelling and assimilation of lidar signals over Greater Paris during the MEGAPOLI summer campaign. Atmos. Chem. Phys. 14, 3511–3532.

Wang, M., Kong, W., Marten, R., et al., 2020. Rapid growth of new atmospheric particles by nitric acid and ammonia condensation. Nature 581, 184–189. https://doi.org/10.1038/s41586-020-2270-4.

Weber, S., Gaelle, U., Calas, A., Chevrier, F., Besombes, J.-L., Charron, A., Salameh, D., Jezek, I., Mocnik, G., Jaffrezo, J.-L., 2018. An apportionment method for the Oxydative Potential to the atmospheric PM sources: application to a one-year study in Chamonix. France. Atmos. Chem. Phys. Discuss. 1 https://doi.org/10.5194/acp-2017-1053. –19.

Weber, S., Uzu, G., Favez, O., Borlaza, L.J.S., Calas, A., Salameh, D., Chevrier, F., Allard, J., Besombes, J.-L., Albinet, A., Pontet, S., Mesbah, B., Gille, G., Zhang, S., Pallares, C., Leoz-Garziandia, E., Jaffrezo, J.-L., 2021. Source apportionment of atmospheric PM10 oxidative potential: synthesis of 15 year-round urban datasets in France. Atmos. Chem. Phys. 21, 11353–11378. https://doi.org/10.5194/acp-21-11353-2021.

Yarwood, G., Rao, S., Yocke, M.A., Whitten, G., 2005. Updates to the carbon bond chemical mechanism: CB05. Final report to the US EPA, RT-0400675 8, 13.

Zhang, Q.J., Beekmann, M., Drewnick, F., Freutel, F., Schneider, J., Crippa, M., Prevot, A. S.H., Baltensperger, U., Poulain, L., Wiedensohler, A., Sciare, J., Gros, V., Borbon, A., Colomb, A., Michoud, V., Doussin, J.-F., Denier van der Gon, H.A.C., Haeffelin, M., Dupont, J.-C., Siour, G., Petetin, H., Bessagnet, B., Pandis, S.N., Hodzic, A., Sanchez, O., Honoré, C., Perrussel, O., 2013. Formation of organic aerosol in the Paris region during the MEGAPOLI summer campaign: evaluation of the volatility-basis-set approach within the CHIMERE model. Atmos. Chem. Phys. 13, 5767–5790. https://doi.org/10.5194/acp-13-5767-2013.

Zhang, Q.J., Beekmann, Matthias, Freney, E., Sellegri, K., Pichon, J.M., Schwarzenboeck, A., Colomb, A., Bourrianne, T., Michoud, V., Borbon, A., 2015. Formation of secondary organic aerosol in the Paris pollution plume and its impact on surrounding regions. Atmos. Chem. Phys. 15, 13973-1399.

Zhang, Y., Favez, O., Petit, J.-E., Canonaco, F., Truong, F., Bonnaire, N., Crenn, V., Amodeo, T., Prévôt, A.S.H., Sciare, J., Gros, V., Albinet, A., 2019. Six-year source apportionment of submicron organic aerosols from near-continuous highly time-resolved measurements at SIRTA (Paris area, France). Atmos. Chem. Phys. 19, 14755–14776. https://doi.org/10.5194/acp-19-14755-2019.

Zhu, S., Sartelet, K., Zhang, Y., Nenes, A., 2016a. Three-dimensional modelling of the mixing state of particles over Greater Paris. J. Geophys. Res. Atmos. 121 https://doi.org/10.1002/2015JD024241.

Zhu, S., Sartelet, K., Healy, R., Wenger, J., 2016b. Simulation of particle diversity and mixing state over Greater Paris. A model-measurement inter-comparison Faraday Discussions 189, 547–566. https://doi.org/10.1039/C5FD00175G.